JAERI-M
83-052

鉄中の水素の溶解および拡散挙動の解析

1983年3月

木　内　　清

日本原子力研究所
Japan Atomic Energy Research Institute

JAERI-M レポートは，日本原子力研究所が不定期に公刊している研究報告書です。
入手の問合わせは，日本原子力研究所技術情報部情報資料課（〒319—11 茨城県那珂郡東海村）あて，お申しこしください。なお，このほかに財団法人原子力弘済会資料センター（〒319-11 茨城県那珂郡東海村日本原子力研究所内）で複写による実費頒布をおこなっております。

JAERI-M reports are issued irregularly.
Inquiries about availability of the reports should be addressed to Information Section, Division of Technical Information, Japan Atomic Energy Research Institute, Tokai-mura, Naka-gun, Ibaraki-ken 319-11, Japan.

編集兼発行　日本原子力研究所
印　　刷　山田軽印刷所

JAERI－M 83－052

鉄中の水素の溶解および拡散挙動の解析

日本原子力研究所東海研究所燃料工学部
木内　清

（1983年2月18日受理）

今迄得られている鉄中の水素の溶解度に関する測定データの多くは，測定の際に表面状態の影響を受けていることが分った。表面効果の少ない手段で測定し，最も低い値を示した測定データのアレニウスプロットは，300～1750Kの温度範囲において，通常の規則固溶体から予想される傾向とは一致せず，単純な直線関係を示さない。このずれの原因は，水素の占有位置の温度変化と関係している。高温では，水素の占有位置として四面体格子間侵入位置と共に八面体のそれも可能となり，温度と共に後者の割合が増大すると仮定したモデルより導いたこの傾向は，実測データのそれとほぼ一致した。

変形過程で導入された格子欠陥と水素との相互作用によって生じる溶解度の増加は，トラップされている水素と，通常の位置にある水素との平衡に対して，Maxwell-Boltzmann統計熱力学を適用したモデルに基いて表現することができる。欠陥による水素のトラッピングのエネルギー深さの解析値として33.9KJ/molを得た。

鉄中の水素の拡散定数Dのアレニウム依存性は，測定者間で大きな異なりを示す。今迄提出されている数多くの測定データの統計処理を行なった結果，バルク中の水素の拡散を反映したD値は，電気化学的な方法とPdを被覆した試料で超高真空装置を用いたH_2ガス平衡法によってのみ得られることが分った。－40～80℃の温度範囲での最も確からしいD値は，

$$D = 7.23 \times 10^{-8} \exp(Q / RT) \quad m^2/sec$$

$$Q = 5.69\ KJ/mol$$

50～550℃の温度範囲でのDは，

$$D = (1 \sim 2.5) \times 10^{-7} \exp(Q/RT)$$

$$Q = 6.70 \sim 7.12\ KJ/mol$$

これらのD間のアレニウス依存性の異なりは，温度の上昇と共に四面体格子間位置を経由しての拡散に対する8面体格子間位置を経由しての拡散の割合が増加することに対応し

ている。

変形した鉄中の水素の拡散は，転位芯によるトラッピングの負の効果と共に転位芯に沿っての〝pipe diffusion〟の寄与を考えた半定量的なモデルに基いて説明することができる。このモデルから計算したDのアレニウス依存性の傾向は，表面効果による影響を受けていない実測データのそれと非常によく一致した。

JAERI-M 83-052

Analysis of Behavior on Solution and Diffusion of Hydrogen in Iron

Kiyoshi KIUCHI

Division of Nuclear Fuel Research,
Tokai Research Establishment, JAERI

(Received February 18, 1983)

It has been shown that a large volume of data for the solubility of hydrogen in iron is affected by spurious surface conditions. Arrhenius plots of solubility data in the temperature range 300 - 1750 K, which are free of such effects, exhibit a temperature variation which, despite the low H-solubility in the entire temperature range, is not consistent with regular mixing statistics. This departure from regular behavior is consistent with the thermal activiation of H atoms into entergetically less favorable octahedral sites as the temperature is increased.

The enhancement in H-solubility caused by the cold deformation of iron can be understood in terms of a simple Maxwell-Boltzmann distribution of H atoms between "normal" lattice sites and "trapping" sites of depth 33.9 kJ/mol.

The sixty-two currently existing sets of data for the diffusivity D of hydrogen through bcc iron exhibit a large degree of mutual inconsistency. Exhaustive statistical analysis of this large data mass has shown that only those data obtained by electrochemical methods and H_2-gas equilibration methods using UHV techniques and Pd-coated membranes are reliable. In the range -40 → 80°C the best representation of D is

$$D = 7.23 \times 10^{-8} \exp (Q/RT) \ m^2/sec$$

where Q = 5.69 kJ/mol.

In the temperature range 50 - 550°C, the best D-representation is,

$$D = [1 - 2.5] \times 10^{-7} \exp (Q/RT) \ m^2/sec$$

with Q in the range 6.70 - 7.12 kJ/mol.

These differing diffusivities are consistent with an increase with temperature of the fraction of H-atoms hopping from octahedral rather than tetrahedral sites.

The problem of H-diffusion in deformed iron has been analysed using a semi-quantitative model in which the retarding effect of trapping sites on the diffusivity is partially compensated by a "pipe" diffusion contribution along dislocations. It is shown that this model is in accord with the diffusivities measured in deformed iron when data not encumbered by spurious surface effects are considered.

Keyworks; Iron and Steels, Hydrogen, Diffusion, Solubility, Deformation Dual Occupancy Model, Pipe Diffusion, Permeation, Absorption, Electrochemical measurement, H_2 Gas-equilibration, Trapping, Dislocation, Surface Defects, Lattice Defects, Grain Boundary

目　　次

Contents

前　置　き

近年原子炉金属材料と水素との相互作用が，軽水炉，多目的高温ガス炉，核融合炉などのほとんどすべての原子炉における工学的な問題として注目されている。鉄鋼材料の水素透過および水素吸蔵による脆化に関する研究を行うことを目的として，昭和56年12月21日より1年間アメリカ合衆国テキサス州のPice大学に留学した。

この期間に同大学材料科学科（Dept. of Materials Science）においてProf. Rex B. McLellanのもとで研究を行い，主として鉄鋼材料中の水素の物理化学的性質および水素脆化の機構を調べ，いくつかの新しい知見を得ることができた。これは，その研究報告の1部である。

1. はじめに

金属材料中の水素の物理化学的性質は，各種原子炉の炉工学上の問題と密接に関係している。特に環境安全性研究に関係したトリチウム透過と原子炉圧力バウンダリー構造材料の使用環境下の健全性に及ぼす水素の影響などでは，既に現実の大きな問題となってきている。金属材料中の水素の溶解と透過に関する測定および理論解析は，水素脆性ならびに水素侵食など実用材料の問題と関連して数多くなされてきている。しかし金属中の水素に関する研究は，基礎的な物性値においても，いくつかの検討課題が残されている。特に実用材料の基金属として重要である鉄の場合，水素の溶解度および拡散速度の測定値は，各測定データ間で大きな不一致を示すことで知られており，この原因の究明が基礎研究の上でも重要な研究課題となってきている。

表1は，Fe，Niなど水素の溶解過程が吸熱反応であるFe基，Ni基などの原子炉構造材料と水素との工学上の問題について，基礎物性および実用上の問題として重要な試験パラメータとの関係を簡略化したものである。本研究では，原子炉構造材料として数多く使用されている鉄基材料を対象として，水素－鉄系の熱力学的および動力学的な問題を実用問題のそれと関連づけて検討してみた。

水素は，他の格子間侵入型元素と比較して，イオン半径（プロトンと考えられている）および化合物形成能が小さい為に，拡散速度が大きく，とりわけBCC金属中での水素の拡散の為に必要な活性化エネルギーは，0.1eV程度と小さく，phononの振動の為のエネルギーに近い。また水素は，他の格子間侵入型元素と大きく異なる点として，金属結晶中でプロトンとしての量子論的なふるまいをすることであり，このため厳密には，波動方程式を用いた解析が必要である。しかし本報告に示すように半経験的な古典モデルによる取扱いでも，十分測定結果を説明でき，工学的な問題にも対応できるものと思われる。

また水素の場合，このように特異な性質を持つ為に，他の格子間侵入型元素や転位などの格子欠陥が存在すると，それらとの相互作用に依って溶解や拡散の性質が大きく変わり易い。また原子炉構造材料の問題を含めて一般に材料内への水素の侵入径路としては，腐食などの表面反応に伴う場合が多い。このために表面状態と密接に関係した水素の脱吸着反応などの素過程が，金属構造材料の水素脆化および水素侵食での律速段階となる場合も少なくない。

実用金属材料の工学的な問題に対して水素の基礎的な物性を基にした本質的な解明を行うためには，基礎的な物性自体を十分明らかにすることと，表1に示したように実用問題で重要な役割りを果たすパラメーターを明らかにすることである。本報告では，この研究の一つとして，まず水素の拡散および溶解の研究に用いられている測定手段および測定データの解析を行ない，鉄中の水素の溶解および拡散について最も確からしい機構を明らかにした。さらに表1中の未知因子のうち，特に塑性歪と水素との相互作用を検討してみた。

表1　金属中の水素の物性と実用材料の工学的問題との関連性

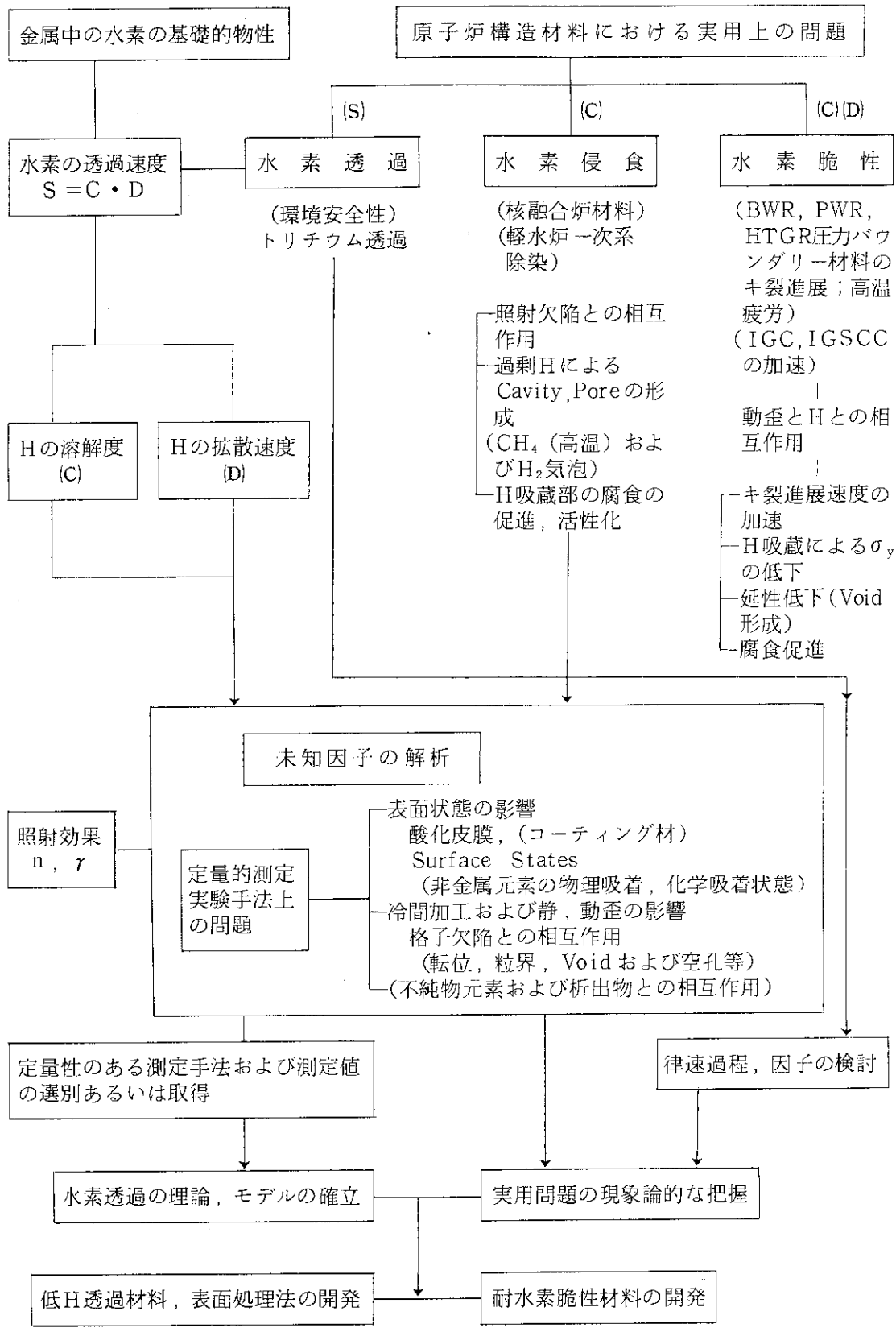

2．焼鈍および変形させた鉄中の水素の溶解度

2.1 概　要

1) α相およびδ相のＢＣＣ構造を持つ鉄中の水素の溶解度は，既に数多く測定されているにもかかわらず，測定データ間の値に異常に大きいばらつきが見られ，この原因および真の水素の溶解挙動は，未だに明らかにされていない。この報告では，今迄出されている測定データを解析して，この原因を調べた。この結果この原因は，試験片の製作段階で作られる表面状態と形成された欠陥の種類と量に依存した表面の影響であることが分った。水素の溶解度が小さい鉄の場合には，低温になる程これらの欠陥がSink sites として大きな役割を果たし，見かけの溶解度を増加させる。この傾向は，測定手段にも関係する。

多くの測定データおよび測定手段を吟味して，最も確からしいバルク中の水素の溶解度の値を抽出し，この値を基に，純鉄への水素の溶解の熱力学的挙動を解析した。この結果，δおよびαのＢＣＣ構造を持つ鉄中の水素の溶解度は，単一の水素の配置状態（例えば四角体格子間侵入位置）を仮定し，単純な規則固溶体の熱力学モデルを基に算出したアレニウム依存性から大きくずれる。このずれは，Ｖ，Nb等，他のＢＣＣ金属で議論されている低温での量子論的な遷移１Ｔ（Sphere）４Ｔ，６Ｔ（Ring）よりも高温で生じ（300Ｋ以上），高温と低温での状態間のエンタルピー変化も大きい。しかしこの傾向は，水素の配置として，低温では四面体位置（Tsites）を優先的に占有するが，高温では，これと共に八面体位置（Ｏ Sites）にも分布するようになることを仮定した" Dual Occupancy モデル " を基にした理論解析結果と非常に良く適合することが分った。

これから純鉄中の水素は，低温ではＴ Sites を占有し高温ではＯ SitesとＴ Sitesの両配置に分布するものと考えられる。この傾向は，本報告のChap.３に示すように水素の拡散定数のアレニウム依存性にもよく対応する。純鉄中の高温における水素の溶解度θ_i^mは次式を用いて表現することができる。

$$\theta_i^m = \theta_i^T \left[1 + \frac{\beta_o}{\beta_T} \exp\left(\frac{\overline{\triangle H}}{kT}\right) \exp\left(-\frac{\overline{\triangle S}}{k}\right) \right] \quad (1)$$

ここで$\overline{\triangle H}$および$\overline{\triangle S}$は，Ｏ sites とＴ sites 間の自由エネルギー△Ｇに関係し，それぞれエンタルピーおよびエントロピーの値の差である。これは，解析の結果次の値が得られた。

$$\overline{\triangle H} = -22.56\,KJ/mol,\ \overline{\triangle S} = 6.0\,K \quad (2)$$

β_oおよびβ_Tは，単位格子中のＯ sites およびTsites の数であり，ＢＣＣ鉄に対しては，$\beta_o/\beta_T = 0.5$である。θ_i^Tは，水素がＴ sites のみ占有すると仮定した場合の水素の溶解度で次式で表現される。

$$\ln(\theta_i^T \cdot T^{7/4}) = \frac{3120 \pm 90}{T} + (3.21 \pm 0.32) \quad (3)$$

水素が実質的にT sitesのみを占有する温度は300 K以下と考えられる。

2) 実用材料で問題となる変形で生じた格子欠陥と水素との相互作用を検討するために，水素の溶解度に及ぼす冷間加工歪の影響を調べた。1）の項に示したように，測定データ間のばらつきの原因として表面状態の影響が大きい事から，まず多くの測定データからこの影響が少ない測定データを抽出し，加工歪と水素の溶解度との依存関係を調べた。この結果次のような点を明らかにすることが出来た。

ⓐ 加工歪と水素との相互作用は，転位と水素とのそれに置き換えて考えることができる。

ⓑ 転位と水素との相互作用としては，水素と転位芯との直接的な相互作用と転位が作る弾性応力場での効果との2つが考えられるが，溶解度に及ぼす主たる効果は，前者に依ることが分った。

ⓒ 加工歪を持つ鉄中の水素の溶解度θ_i^{cw}は，Maxwell－Boltjmann統計熱力学を適用することにより，無歪結晶中の水素の溶解度θ_Lの関数として次式のように表現することができる。

$$\theta_i^{cw} = \theta_L \left[1 + \alpha \cdot \phi \cdot \exp(\triangle H^* / kT)\right] \quad (4)$$

ここで$\alpha = \exp(-\triangle S^*/k)$，$\triangle H^*$および$\triangle S^*$は，$\triangle G^* = \triangle H^* - T \cdot \triangle S^*$で表わされ，$\triangle G^*$は通常の格子間位置の水素と，転位に拘束された水素（Trapping sites）との自由エネルギーの差である。ϕは，欠陥濃度であり；転位の数φ'（m^{-2}）に比例する。θ_Lとして単結晶中の水素の溶解度を用い，いくつかの異なる加工歪を持った試料のθ_i^{cw}の値とを比較した結果，ϕとϕ'の間に次の依存関係があることを見出した。

$$\alpha \cdot \phi = 2.04 \times 10^{-16} \phi' \quad , \quad \triangle H^* = 33.1 \text{ KJ / mol}$$

4) 式の依存関係から得た計算値は，広範囲の塑性歪域に渡り，実測データと非常によい一致を示す。また上記のϕ'の係数の値は，転位が格子と交叉する数から得た計算値4.31×10^{-16}と非常によく対応する。これはほぼ転位線に沿って2格子間隔当りに1つの欠陥サイトが存在することを意味する。この傾向は，Pdなど水素の溶解度が大きく，また発熱反応型の水素吸蔵を示す金属のそれと大きく異なる。これらの金属では，水素と転位の弾性場との相互作用の効果も大きいと考えられ，転位が水素を凝集する効果が非常に大きい。

2.2 General concepts

Recent years have witnessed a large volume of research work directly connected with the thermodynamic and kinetic behavior of the hydrogen-iron system [1-22]. One reason doubtless lies in technological importance associated with the degradation of ferrous engineering materials resulting from hydrogen absorption. A more fundamental motivation lies in the fact that over the years the generation of more data has, by and large, seemingly contributed to the existing confusion surrounding this basic metallurgical binary system. The data of different investigators often show alarming mutual discrepancy in the solubility, and especially in the hydrogen diffusivity [1-4], in the low-temperature region. Much work has been centered on analyzing the anomalies at low temperature in terms of trapping effects associated with interactions between hydrogen and defects produced during pretreatments or existing at the surface of the iron [23-29], or associated with the essential properties of the iron lattice at low temperatures [30].

The initial problem considered in this report concerns the relationship between the experimental methods used in obtaining thermodyanamic and kinetic data in the Fe-H system to the generation of real and apparent anomalies in experimental results. Solubilities at high temperatures are usually measured by simple procedures [6,7], involving the equilibrate-quench-analyze technique and are less prone to errors than are low-temperature diffusivity measurements [1]. However, it is always difficult to eliminate the effects of surface defects resulting from differing pretreatments. Many investigations [23-29] have shown the existence of surface sites acting as traps for hydrogen and which persist even after annealing. It is clear that surface voids and microcracks formed during heavy cold working are not removed by annealing [26,27], but other problems arise due to inappropriate surface finish. If surface finishing involving

mechanical polishing is performed subsequent to annealing, thin Beilby layers may be produced [31-33]. Surface finishing by electrochemical polishing after annealing or Pd coating can obviate this problem [20-22].

Surface cleaning may be effected by vacuum annealing, but this is not always appropriate since interfering surface conditions may be produced depending on the vacuum annealing conditions (oxygen) [34]. Ion sputtering techniques can also cause surface effects [36,37] and their formation has also been ascribed to the repeated use of the same sample [35].

Another interfering factor is sample shape. Surface trapping in thin membranes obviously leads to anamalously high solubilities.

The effect of deformation on the solubility of hydrogen in iron is of great technological importance [38,39]. Voids are formed in highly deformed iron, usually only in surface layers, but the most important result of deformation is of course a high dislocation density. Much work has centered on hydrogen-dislocation interactions in deformed iron [24], [40-43]. However, as will be pointed out later in this paper, these analyses are hampered by the very nature of the uncertainties in the experimental data itself.

Even though crystal grain structure has been shown to have a large effect on H solubility in Ni and Co at high temperatures [44], its effect in Fe has been detected only at low temperatures [41]. Thus metallographic features, and the trapping of H at impurity atoms [45-47], appear to be important only at low temperatures [41].

A further consideration relates to the question of what the term "anomaly" infers anyway. The behavior of H in bcc metals is often explainable only in non-classical terms (especially the Group V metals [48,49]) and non-classical considerations may dictate the behavior of H in the defect-free iron lattice in such a manner that classical Arrhenius solubility or diffusivity relationships are not to be expected anyway. It is fairly clear [50,51] that H occupies

tetrahedral (T) sites in bcc iron at low temperatures, but the situation at higher temperatures is far from clear. Let us recapitulate the causes of the experimental uncertainties in experimental data in the Fe-H system and point out the aims of this report by stating the following sources of uncertainty.

(1) Experimental uncertainties related to defects in specimens either formed during pretreatments or arising due to experimental conditions.

(2) Differences in metallographic structure and impurity levels.

(3) Non-Arrhenius behavior in the temperature dependence of the hydrogen solubility of H in bcc iron in the absence of the two groups of effects listed above (i.e. behavior in a "perfect" bulk lattice).

After discussing each of these three areas we will discuss the effect of deformation on hydrogen solubility in iron using a simple model for the effects of H-dislocation interactions.

2.3 HYDROGEN SOLUBILITY IN WELL-ANNEALED IRON

2.3.1 Analysis of Scatter in Experimental Data

The first task is to elucidate the "true" hydrogen solubility in α-iron by considering the available solubility data in terms of the sources of error outlined previously in section I.

Normal experimental error (random errors) are usually expressed in terms of a statistical distribution such as a Gaussian function [53]. However, when bulk or surface defects having high binding energies with H occur, the experimental data will exhibit some defect-related tendency overriding the usual random errors, and this tendency will be more pronounced at low temperatures [20-23] due to the exothermal nature of the H-defect interaction.

First let us show of the available solubility data. This is given in Fig. (1). The concentration unit θ_i is the number of H-atoms per Fe atom.

Fig (1) reveals several obvious features. Firstly it is clear that the degree of scatter increases rapidly as temperature decreases. Secondly the data in general (i.e. weighting each data set equally) do not conform to an Arrhenius plot of ln θ vs. 1/T. The high-temperature data (> 225°C) are shown in a magnified form in Fig. (2). Except for the lowest-temperature points given in Fig. (2) ($10^4/T < 20$), all the data were obtained by the H_2 gas equilibration method. In this high-temperature region there is a clear tendency to a positive deviation from Arrhenius behavior at ~700°C, corresponding to a H-solubility of $\sim 5 \times 10^{-5}$. This deviation is not considered to be due to random error, but rather to some overriding mechanism. Let us consider the following five possible mechanisms:

a) Intrinsic interactions between H-atoms and interstitial sites or vacancies in the iron lattice.

b) The effect of metallogrpahic factors such as grain boundaries and impurities.

c) Deformation-related defects, e.g. dislocations.

d) Trapping at surface sites.

e) Intrinsic non-Arrhenius behavior, i.e. when the nature of the interaction between H-atoms and the defect-free bulk iron lattice is such that Arrhenius behavior is not to be expected in the H-solubility.

Now it is clear [20,21,23,41] that the mechanisms (a), (b) and (c) are important at lower temperatures, but are not causative mechanisms in the temperature range in fig (2), i.e. above 300°C. The vacancy concentration is too low to represent a reasonable trapping mechanism [8]. Moreover the solubility at this temperature, $\sim 2 \times 10^{-5}$, is such that departures from Arrhenius behavior require very deep trapping sites or high concentrations of trapping

sites [40,44] having at least the H-atom binding energy of a dislocation, i.e. about 33 kJ/mol [25, 53]. Thus let us limit our considerations in this temperature range to mechanisms (d) and (e)

Consider first the surface states. It is essential to consider the sample preparation process, and in particular the final stage of preparation. A careful perusal of all the reports from which the data of fig. (2) were taken shows that the minimum solubilities were found when the final surface treatment was electrochemical polishing. This procedure was followed in only a few [20,21] of the cases, whilst the most usual procedure involved vacuum annealing after heavy cold deformation or mechanical abrasion using emery or diamond paste. The work of Samuels using a variety of metals [31-33] clearly shows that mechanical abrasion produces Beilby layers without exception. Such layers contain large concentrations of voids and dislocations. Since the equilibration samples, particularly at low temperatures, are usually thin membranes, mechanical polishing leads to an enhanced solubility. Structures resulting from heavy cold deformation, and also Beilby layers, cannot be completely anihilated by vacuum annealing. In general thin layers of fine-grained structure result from annealing, but it has been shown [51] that absorbed oxygen acts as an inhibitor toward grain boundary migration. It may be impossible to differentiate between the effects of a fine-grained post-recrystallized layer and the effects of H-O interactions in the surface layers. The penetration of oxygen into the surface cannot be inhibited even under ultra high vacuum annealing conditons [67]. The absorption of O occurs even at 10^{-8}Pa and the coverage fraction of active residual oxygen reaches almost unity under high-vacuum conditions (10^{-3} - 10^{-4} Pa). The concentration of oxygen dissolved in surface layers under given thermal treatment conditions depends on the intrinsic oxygen solubility. The sequence for the metals

Fe, Co and Ni at 900°C [55-58] is as follows:

$$\underset{\sim 0.01 \text{ at. \%}}{\text{Fe}} < \underset{\sim 0.03 \text{ at. \%}}{\text{Co}} < \underset{\sim 0.05 \text{ at. \%}}{\text{Ni}} \qquad (1)$$

All of these metals exhibit an anomalous H-solubility enhancement at low temperatures, which, at a given temperature, is in the same sequence as equ. (1). This is shown graphically in fig (3). The minimum solubilites are taken from the extrapolated high-temperature data [55-58] and the maximum solubilities are as measured. It must however be pointed out that the influence of grain boundaries upon H-solubility is not clearly understood [67] and it may be that O-diffusion from the surface layers along grain boundaries plays an important role in the anomalous enhancement of H in these metals. Similar effects have been observed in vacuum annealing in the Fe-N system [69]. As a final comment, let us point to the dramatic effects produced by Pd-coating in diminshing surface effects [68].

Dissolved oxygen is not reduced by H under equilibrium conditions and the repeated use of the same sample with oxygen exposure can lead to a drastic reduction in permeability [61].

To summarize these considerations we conclude that the most reliable solubility data are obtained by the gas-equilibration method using electrochemical surface preparation . However, as shown in Fig. (1), there is a clear general increase in θ_i at low temperatures, in respect to the Arrhenius behavior at high temperatures, and this may be at least in part due to the intrinsic nature of the Fe-H interaction and not to surface effects. This will be discussed in the following section.

2.3.2 Theoretical Treatment of Hydrogen Solubility in Iron

The solubility of a diatomic gas can be written in the general form [70],

$$\theta = \frac{\beta P^{1/2} \psi}{T^{7/4}} \exp\left[-\frac{\bar{H}_i - 1/2\, E_o^D}{kT}\right] \exp\left(\frac{\bar{x}_i^{xs}}{k}\right) \qquad (2)$$

where $-E_o^D$ is the dissociation energy of the H_2 molecule at 0 K per atom, ψ is a known [70] constant, β the number of interstitial sites per metal atom, and $\bar{H}_i$ and $\bar{S}_i^{xs}$ are the partial enthalpy and excess entropy of the dissolved interstitial atoms. The gas pressure is P. This equation is completely valid, and shows that, provided $\bar{H}_i$ and $\bar{S}_i^{xs}$ do not vary with either concentration or temperature, plots of ln θ vs 1/T will not be linear due to the term (7/4) ln T. Furthermore the non-linearity will be more pronounced in the temperature range ΔT when T is low so that (7/4) ln (ΔT/T) is proportionately large.

Now in certain interstitial solid solutions measured data show that both $\bar{H}_i$ and $\bar{S}_i^{xs}$ are indeed constant over long temperature ranges. The b.c.c. Fe-C system is a prime example [71]. However the protonic nature of H dissolved in metals [48,49] leads to the idea that it may not be appropriate to regard the dissolved H atom in the traditional sense of a bound oscillator located in a single type of interstitial site, nor even appropriate to consider that the dissolved H-atoms possess only vibrational degrees of freedom in the metal lattice.

The discussion of the "correct" model concept for bcc Fe-H solutions must start with a selection of the "best" solubility data, i.e. such data which are free from the exterraneous factors giving rise to solubilities not reflecting the intrinisc H-lattice interaction. These "best" data have been selected according to the discussion on the previous sections by taking the following data groups:

(a) High-temperature data obtained above 873K

(b) Low-temperature data obtained with due cognizance to correct surface treatment.

A plot of these data in the form of ln ($\theta\ T^{7/4}$) vs. 1/T is given in Fig. (4). The data were taken from the references given on Fig. (4).

It can clearly be seen that the plot is not linear. The simplest explanation of the curvature found is that proposed by da Silva and McLellan [7], according to which the H-atoms act as bound oscillators in interstitial sites in the entire temperature range. At low temperatures the tetrahedral sites are more stable, but as T increases entropic factors cause an increasing fraction of octahedral sites to become occupied. It has been shown [7], that in this model the chemical potential of the H in the solid is given by

$$\mu_i = kT \ln \frac{\theta_i^m}{\left\{ \frac{\beta^o}{\beta_T} \exp\left(\frac{\Delta\bar{H}}{kT} \right) \exp\left(- \frac{\Delta\bar{S}}{k} \right) + 1 \right\} \beta_T} + \bar{H}_i^T - T\bar{S}_i^T \qquad (3)$$

where the superscript "m" denotes the "mixed" i.e. dual-occupancy state, $\beta_{o,T}$ denotes the number of O or T sites per lattice atom (3 and 6), $\bar{H}_i^T$ and $\bar{S}_i^T$ are the partial enthalpy and excess entropy in the T-sites (i.e. at $T \to 0$) and, with obvious notation, $\Delta\bar{H} = \bar{H}_i^T - \bar{H}_i^o$ and $\Delta\bar{S} = \bar{S}_i^T - \bar{S}_i^o$. The solubility θ_i^m in the "mixed" state, i.e. at T increases, is given by [7]

$$\frac{\theta_i^m}{\theta_i^T} = 1 + \frac{\beta_o}{\beta_T} \exp\left(\frac{\Delta\bar{H}}{kT} \right) \exp\left(-\frac{\Delta\bar{S}}{k} \right) \qquad (4)$$

In equ. (4), θ_i^T represents the (low temperature) solubility corresponding to T-occupancy only.

A least-squares regression was applied to the data of fig. (4). The best values of $\Delta\bar{H}$ and $\Delta\bar{S}$ were $\Delta\bar{H} = -22.56$ kJ/mol and $\Delta\bar{S} = -6.0$ k. The curved solid line in fig. (4) illustrates the variation of ln ($T^{7/4}\ \theta_i$) vs 1/T calculated from the above values of $\Delta\bar{H}$ and $\Delta\bar{S}$ and the linear fitting results

(lower dashed line) obtained at T < 300 K, i.e.

$$\ell n \left(\theta_1^T \; T^{7/4} \right) = - \frac{3120 \pm 90}{T} + (3.21 \pm 0.32) \qquad (5)$$

It can be seen that the curved solid line gives a satisfactory representation of the measured solubility.

2.4 EFFECT OF MECHANICAL DEFORMATION ON THE SOLUBILITY OF HYDROGEN IN BCC IRON

The change in hydrogen solubility in iron with degree of cold deformation depends on the concentration of lattice defects thus introduced and their interaction with hydrogen. Non-equilibrium defects are removed upon annealing, accompanied by the formation of secondary defects or, at high temperatures, recovery. These complex phenomena are a function of annealing temperature and time. However, at sufficiently low temperatures, it is possible to consider the system Fe + H + defects as representing quasi-static equilibrium and treat the effect of deformation of H-solubility thermodynamically.

In comparison with the noble metals, which have low vacancy formation energies, and the tendency to form stacking faults or Frank Loops [66], the defect structure in bcc iron is stable at low temperatures and the bulk of the literature devoted to the H-solubility enhancement due to cold work has dealt with the interaction between H-atoms and quasi-stable defects. Defects associated with grain boundaries and dislocations can be treated as having similar properties [41] with the exception of having a differing H-defect binding energy [23]. On the other hand, several investigators have discussed H-solubility in heavily deformed and annealed iron containing H in voids, micro-cracks, and subsurface layers formed either during annealing or cold-work itself [23,29].

In this work, we will discuss H-solubility enhancement due to dislocation-related sites in moderately cold-worked iron. As in the previous discussion, only experimental data will be used in which electrochemical polishing was used to remove the defect-rich surface layers [20,23].

The calculation of H-trapping at dislocations is, of course, an old topic. Hirth and Carnahan [72] have performed a rigerous calculation of the interaction between H-atoms and the stress-field of a dislocation using the isotropic elastic approximation. However, statistical mechanical calculations involving more than two energetically distinct sites are extremely cumbersome and statistical approaches have usually been restricted to two-site models (i.e. "normal" sites and "trapping" sites). The well-known treatments of Oriani [24], Koiwa [73], and McLellan [40,74] may be quoted. A discussion of the relative merits of these calculations will not be given here since they will be discussed fully in respect to the kinetics of the H-Fe system to be treated in report II of this series. Before commencing the quantitative treatment of enhanced solubility let us make it clear that, in comparing measured solubilities to model predictions, we will use only data obtained in experiments where the surface treatment conforms to the requirements laid down in the previous section.

Consider an iron sample containing N iron atoms and Nϕ trapping sites. Of the N_I H-atoms, N_B are located in "defect" sites and N_L in normal sites (i.e. T-sites at low temperatures). The distribution function giving the temperature dependence of N_L and N_B is a Maxwell-Boltzmann distribution given by[40],

$$\frac{(N\phi - N_B)}{N(1-\phi) - N_L} \cdot \frac{N_L}{N_B} = X, \qquad (6)$$

where $X=\exp(\Delta G^*/kT)$ = and ΔG^* is the depth of the trapping site well with respect to the normal T-site. Now the limit where $N\phi >> N_B$ and $1>>\phi$ this can

be written in the simple form,

$$N_B = N_L \quad \phi X^{-1} \tag{7}$$

Let us write $\Delta G^* = \Delta H^* - T\Delta S^*$, and, assuming ΔS^* is temperature-invariant, the total H-concentration in the defect-containing material $\theta_i^{CW} = (N_B+N_L)/N$ is simply,

$$\theta_i^{CW} = \theta_L \left[1 + \alpha\phi \exp\left(\frac{\Delta H^*}{kT}\right)\right] \tag{8}$$

where $\alpha = \exp(-\Delta S^*/k)$ and $\theta_L = N_L/N$. The defect density ϕ represents trapping sites at dislocation cores or close thereto. The physical meaning of ϕ will be discussed more fully later (second paper of this series).

Let us compare the solubility equation (8) with the data measured by Yamakawa et. al [20,21]. These authors used appropriate surface treatments and measured the enhanced H-solubility in cold worked mild steel. They obtained dislocation densities ϕ' by direct transmission electron microscopy and correlated x-ray diffraction data [21]. The variation of $\ln \left[(\theta_i^{CW}/\theta_L) - 1\right] / \phi'$ vs $1/T$ are shown in fig. (5). The least-squares regression to these data lead to the parameters ΔH^*=33.9 kJ/mol and $\alpha\phi = 2.04 \times 10^{-16}\ \phi'$. Now assuming for simplicity that each dislocation line yields one trapping site per unit cell length along the dislocation line then the number of sites per metal atom is

$$\phi = \phi' \frac{d\ N_o}{M\ a}$$

where d is the density, N_o is Avogadro's number, M is the atomic weight of Fe, and a is the lattice parameter. This simple calculation yields the result $\phi = 4.31 \times 10^{-16}\ \phi'$. This is remarkably good accord with the previous finding of $\alpha\phi = 2.04 \times 10^{-16}\ \phi'$ since there is no reason to suppose that $\exp(-\Delta S^*/k)$ is

not small. The value of $\Delta H^* = 33.1$ kJ/mol may be compared with that found recently by Kummick and Johnson [42] [59.9 kJ/mol], that deduced by Gibala [25] [26.79 kJ/mol], and that given by Oriani [24] [27.2 kJ/mol]. Although all the these estimates are close, it must be emphasized that they are all subject to uncertainties in ΔS^* since in fact in reality the quantity ΔG^* is estimated experimentally when H-enhancement is measured isothermally as a function of degree of deformation.

The degree of coincidence between equ. (8) and the data of Yamakawa et.al. [20,21] is shown in Fig. (6). This plot shows the values of (θ^{CW}/θ_L) vs 1/T calculated from equ. (8) using the parameters ΔH^* and $\alpha\phi$ given. The symbols give the actual values of (θ^{CW}/θ_L) for given dislocation densities taken from the measured data. The condition $N\phi > N_B$ i.e. $\phi > \theta_B$ where $\theta_B = N_B/N$ is satisfied. The value of θ_L taken from fig. (1) at 300°C is $\sim 5 \times 10^{-8}$. Using this value of θ_L and the values of $\alpha\phi$ and ΔH^* given shows that $\phi/\theta_B \approx 27.5$ for both the maximum dislocation densities given by Yamakawa et. al.

To summarize these results, it may be stated that,when due cognizance is given to the elimination of misleading surface effects, the enhancement in H-solubility in iron due to trapping sites may be explained by the simple Maxwell-Boltzmann relation (8). This conclusion however must be in accord with the kinetic behavior of the Fe-H system. In considering this behavior we must again, of course, apply the same criteria for data selectivity and give special care to interfering surface effects. This problem will be considered in the next paper in this series.

2.5 CONCLUSIONS

[1] The large mass of solubility data available for well-annealed iron exhibits both mutual discrepancies and deviations from simple mixing behavior leading to a departure from linearity in the Arrhenius plot of the solubility vs. reciprocal temperature.

[2] The mutual discrepancy in the data may be largely resolved by considering only data in which, especially at low temperatures, the interfering effects arising from the surface of the samples have been obviated.

[3] The "best" data conforming to [2] above still shows non-linearity in the Arrhenius plot of solubility vs. reciprocal temperatures. This observed non-linearity may be explained in terms of a model in which H-atoms occupy the tetrahedral sites in the bcc lattice at low temperatures, but can simultaneously occupy both tetrahedral and octahedral sites at high temperatures.

[4] Provided the density of trapping sites is greater than that of trapped H-atoms, the enhancement of the H-solubility of deformed iron can be explained by a simple Maxwell-Boltzmann distribution of H-atoms between "normal" lattice sites and "defect" sites produced by deformation. The depth of such "defect" sites is 33 kJ/mol.

[5] In order to account for enhanced solubility due to deformation, only such data must be used in the analysis for which cognizance is given to the elimination of interfering surface effects.

[6] The conclusions reached concerning the solubility of hydrogen in well-annealed and cold-worked iron must be such that the models proposed are in accord with the kinetic properties of the iron-hydrogen system. This will be considered in the second paper of this series.

REFERENCES

[1] J. Völkl and G. Alefeld, Diffusion in Solids (Edited by A.S. Nowick and J. J. Burton). Academic Press, New York. Chap. 5, 231 (1975).

[2] H. Schenk and K. W. Lange, Arch. Eisenhüttenw 37, 739 (1966).

[3] J. D. Fast, Interaction of Metals and Gases (1965).

[4] O. D.Gonzalez, Trans. AIME 245, 607 (1969).

[5] R. A. Oriani and O. D. Gonzalez, Trans. AIME 239 1041 (1967).

[6] J.R.G. DaSilva and R. B. McLellan, J. Less-Common Metals 50, 1 (1976).

[7] J.R.G. DaSilva and S. W. Stafford and R. B. McLellan, J. Less-Common Metals 49 407 (1976).

[8] A. Sieverts, Z. Phys. Chem. 77, 591 (1912).

[9] A. Sieverts, G. Zapf and H. Moritz, Z.Phys. Chem., Teil A 183, 19 (1938).

[10] A. Sieverts and H. Hagen, Z. Phys. Chem. Teil A 155 314 (1931).

[11] Luckmeyer-Hasse and H. Schenk, Arch. Eisenhüttenw 6, 209 (1932).

[12] E. Martin, Arch. Eisenhüttenw 3 407 (1929).

[13] M. H. Armbruster, J. Amer. Chem. Soc. 65, 1043 (1943).

[14] J. H. Andrew, H. Lee and A. G. Quarrell, J. Iron Steel Inst. 16 181 (1942).

[15] J. H. Andrew, H. Lee and A. G. Quarrell, Iron and Steel 16 140 (1942).

[16] W. Baukloh and R. Müller,Arch. Eisenhüttenw 11 513 (1937).

[17] J. Pihlstrand, Jernkontrets. Ann. 121 219 (1937).

[18] T. Iwase and K. Fukushima, Science Reports, Tohoku Imp. Univ. 27 162 (1938).

[19] M. R. Louthan, P. G. Derrick, J. A. Donovan, and G. R. Caskey. Eff. Hydrogen. Behav. Mater. Proc. Int. Conf. Moran, Wyoming, p. 337, AIME, New York (1978).

[20] K. Yamakawa, T. Tsuruta and S.Yoshizawa, Boshoku Gijutsu 30 443 (1981).

[21] K. Yamakawa, T. Tsuruta and S. Yoshizawa, Boshoku Gijutsu 30 501 (1981).

[22] N. R. Quick and H. H. Johnson, Acta. Metall. 26 903 (1978).

[23] W. Y. Choo and Jai Young Lee, Metall. Transactions A 13A 135 (1982).

[24] R. A. Oriani, Acta Metall. 18 147 (1970).

[25] R. Gibala, Trans. Metall. Soc. AIME 239 1574 (1967).

[26] D. F. De Sante and A. S. Tetelman, Trans. Metall. Soc. AIME 242 1473 (1968).

[27] J. G. Harhai, T. S. Viswanathan and H. M. Davis, Transactions of the ASM 58 210 (1965).

[28] H. J. Koenig and K. W. Lange, Arch. Eisenhüttenw 46 237 (1975).

[29] J. Chene, J. Galland and P. Azou, Hydrogen Met. Proc. Int. Congr. 2nd. 1A3 (1977).

[30] K. Ono and L. A. Rosales, Trans. AIME 242 244 (1968).

[31] L. E. Samuels and G. R. Wallwork, Inst. Metals 85, 177 (1956).

[32] L. E. Samuels and G. R. Wallwork, J. Iron andSteel Inst. 186 211 (1957).

[33] L. E. Samuels and G. R. Wallwork, J. Inst. Metals 86 43 (1957).

[34] P. A. Redhead, J. P. Hobson and E. V. Kornelsen, The Physical Basis of Ultra high Vacuum, Chapman and Hall, London (1968).

[35] P. L. Chang and W. D. G. Benett, J. Iron Steel Inst. 170 205 (1952).

[36] T. Yamashina and H. E. Farnsworth, Ind. Eng. Chem. Proc. Res. Rev. 2 34 (1963).

[37] H. E. Farnsworth and R. F. Woodcock, Adv. in Catalysis 9 23 (1957).

[38] R. A. Oriani and P. H. Josephic, Acta Metall. 22 1065 (1974).

[39] J. A. Donovan, DP-MS-75-42 (ERDA) (1975).

[40] R. B. McLellan, Acta Metall. 27 1655 (1979).

[41] H. Hagi, Y. Hayashi and N. Ohtani, Trans. JIM 20 349 (1979).

[42] A. J. Kumnick and H. H. Johnson, Acta Metall. 28 33 (1980).

[43] J.C.M. Li and Y. T. Chou, Trans. AIME 245 1960 (1969)

[44] S. W. Stafford and R. B. McLellan, Acta Metall. 23 1463 (1974).

[45] C. Baker and H. K. Birnbaum, Acta Metall. 21 865 (1973).

[46] J. Englhard, J. Phys. F., Metal Phys. 9 2217 (1979).

[47] K. Faber and H. Schultz, Scripta Met. 6 1065 (1972)

[48] H. I. Birnbaum and C. P. Flynn, Phys. Rev. Lett. 37 25 (1976).

[49] H. Sugimoto and Y. Fukai, Phys. Rev. B 22 670 (1980).

[50] J. P. Wallace, Scr. Met. 12 791 (1978).

[51] A. Seeger, Phys. Lett. A 58A 137 (1976).

[52] P. R. Berington, Data Reduction and Error Analysis for the Physical Sciences, McGraw-Hill, New York (1969).

[53] Y. Sakamoto and J. Equchi, Proc. Japan Congr. Met. Res. 19 91 (1976).

[54] O. Kubachewski and V. E. Hopkins, Oxidation of metals and alloys, Butterworths, London (1962).

[55] J. L. Meijering, Acta Metall. 3 157 (1955).

[56] J. H. Swisher and E. T. Turkdogan, Trans. AIME 239 427 (1967).

[57] A. U. Seybolt, ASM Metals Handbook 1231 (1948).

[58] A. U. Seybolt, Trans. AIME 117 156 (1935).

[59] H. Schenck and H. Taxhet, Arch. Eisenhüttenw 30 661 (1959).

[60] W. Geller and Tak-Ho Sun, Arch. Eisenhüttenw 21 423 (1950).

[61] P. L. Chang and W. D. G. Benett, J. Iron Steel Inst. 170 205 (1952).

[62] J. Horiuchi and T. Toya, Chemisorbed Hydrogen, Solid State Surface Science Vol. I (1969).

[63] F. T. Wall, Chemical Thermodynamics, W. H. Freeman, San Francisco, (1974).

[64] R. Fowler and C. J. Smithells, Proc. Roy. Soc. A160 37 (1937).

[65] R. B. McLellan, et.al., Trans. Metall. Soc. AIME 233 1938 (1965).

[66] A. A. Hussein, Metall. Trans. A 6A 424 (1975).

[67] R. B. McLellan and S. W. Stafford, Acta Metall. 22 463 (1974).

[68] K. Kiuchi and R. B. McLellan, in preparation.

[69] M. Doyama and J. S. Koehler, Acta Metall. 24 871 (1976).

[70] R. B. McLellan, "Phase Stability of Metals and Alloys." McGraw-Hill, New York (1966).

[71] W. W. Dunn and R. B. McLellan, Met. Trans. 2, 1079 (1971).

[72] J. P. Hirth and B. Carnaham, Acta Metall. 26 1795 (1978).

[73] M. Koiwa, Acta Metall. 22 1759 (1974).

[74] R. B. McLellan, Scripta Metall. 15 1251 (1981).

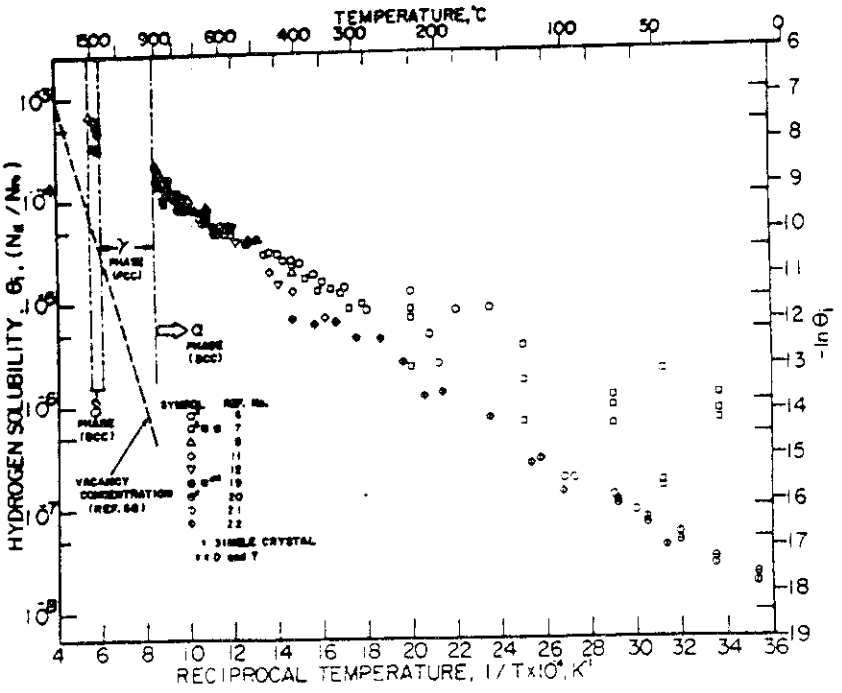

Fig.(1) Hydrogen solubility in BCC iron as a function of temperature.

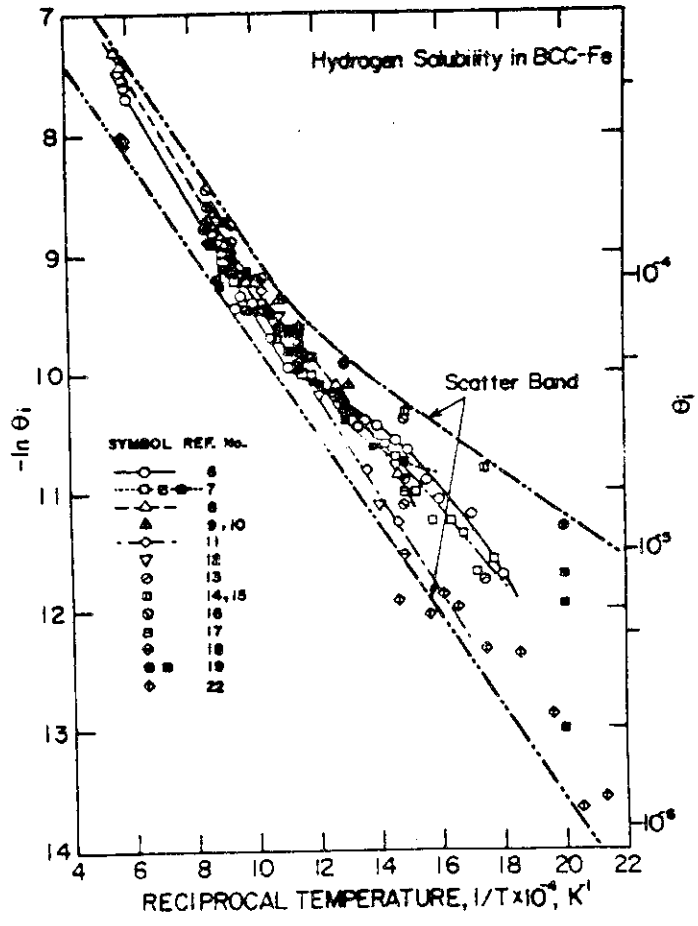

Fig.(2) Hydrogen solubility in BCC iron in the high temperature region. The symbols used for different investigations are consistent with Fig.(1).

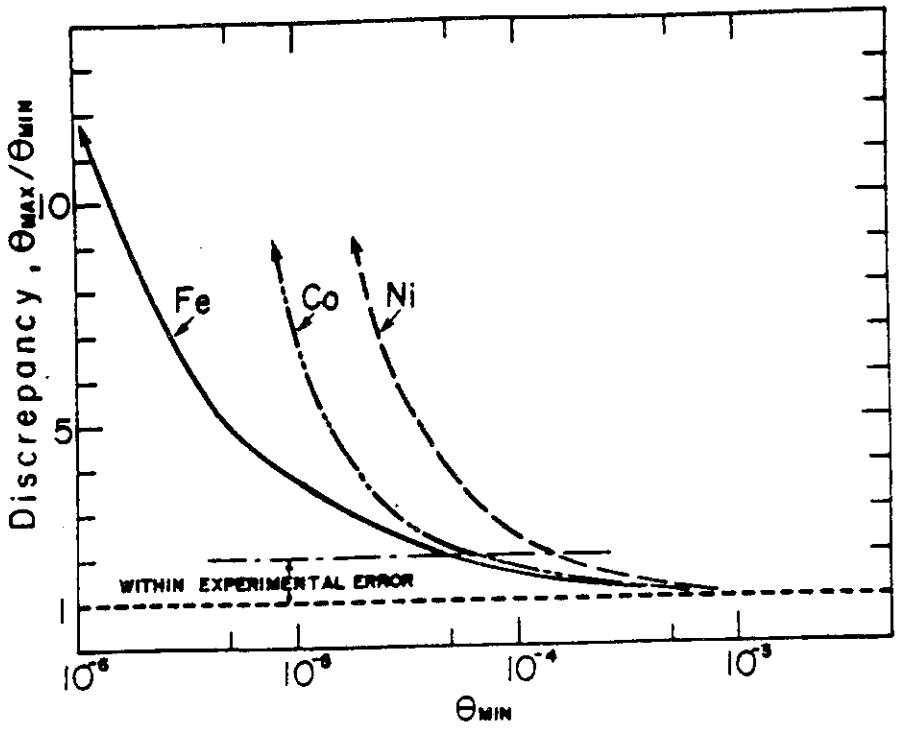

Fig.(3) The low temperature H-solubility enhancement in Ni, Co, and Fe. The discrepancy is the ratio of 0, measured at high temperatures and extaporated down to the given values of 0_{min}. The 0_{max} is taken from actual low-temperature data.

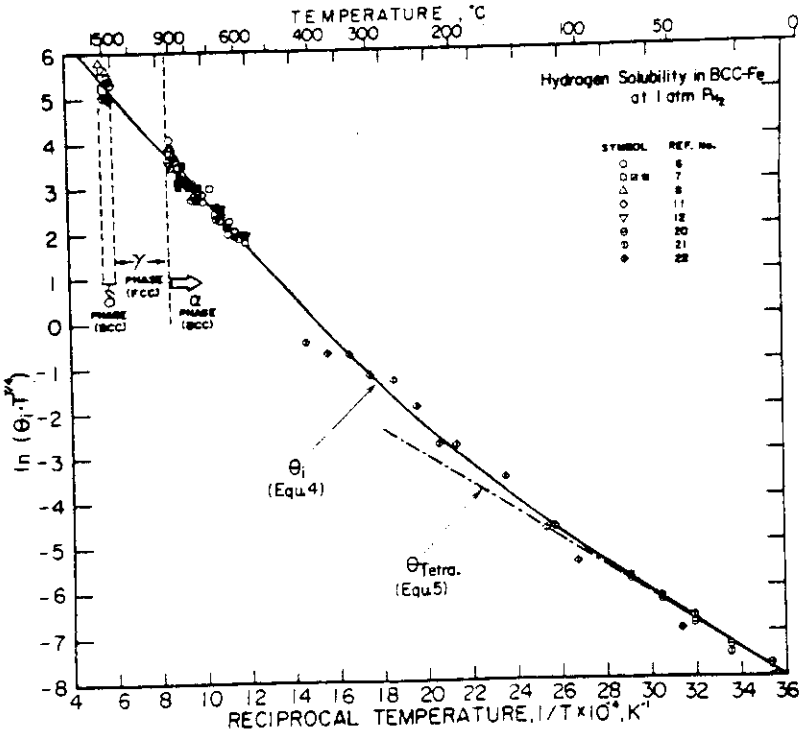

Fig.(4) Plot of ln ($\theta_i \cdot T^{7/4}$) vs. 1/T for hydrogen in BCC iron. The data points given (symbol communality between Figs.(1,2 and 4)) are selected using the criteria discussed in the text so as to represent the most reliable solubility information.

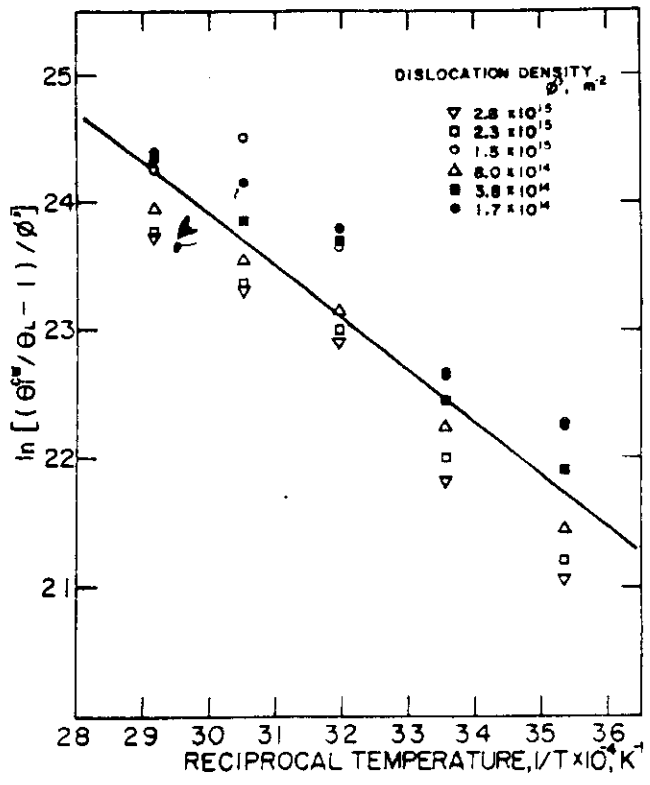

Fig.(5) Plot of the function ln [(θ_i^{CW} / θ_L)-1] / ϕ'^2 vs. 1/T for cold worked mild steel. The different symbols refer to differing dislocation densities as shown on the diagram.

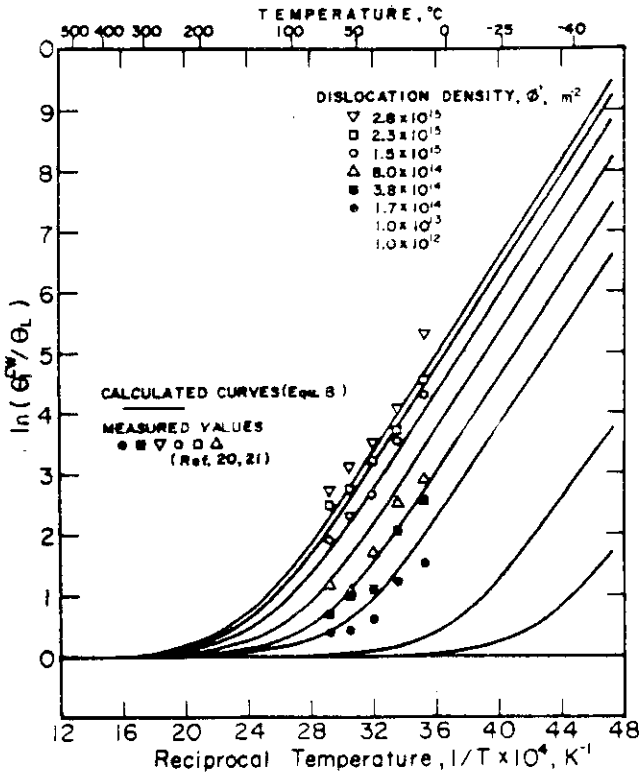

Fig.(6) The solubility enhancement ratio θ_i^{CW} / θ_L as a function of 1/T for differing dislocation densities according to Yamakawa et. al. [20, 21] . The solid lines represent caluculated values.

3．焼鈍および変形させた鉄中の水素の拡散

3.1 概　　要

1） 拡散速度は，金属中の水素の物理化学的性質の中でも実用材料の水素脆化の問題と関連した最も重要な物性値である。しかし鉄に関してみると，焼鈍した純鉄中の水素の拡散速度でさえも研究者間の測定値に異常なばらつきが見られ，その原因および拡散機構の解明が長年の研究課題となってきた。多くの拡散定数の測定値をアレニウスマップ上にプロットしてみると見かけ上常温付近で急激に異常に低い値に収斂する傾向が見られ，ばらつきも低温側程増大する。この為真性 trapping，表面状態の影響および歪などの格子欠陥による偽性Trapping などの観点からこの原因が検討されてきた。この報告では今迄得られている測定データについて測定手段，表面処理条件などに関連づけた統計的な解析を行ない，この原因を解明し次に示す知見を得た。

ⓐ 測定データ間のばらつきは，測定手段および試料の作成条件と深いかかわりを持っており，真性Trapping（H－H間相互作用など），試験片の組成や金属組織学的因子(粒界など)が水素の拡散に及ぼす効果は少ない。

ⓑ 表面状態あるいは歪による影響を極小とする事が可能な測定手段は，電解研磨を施した試料を用いた電気化学的測定法（低温）および Pd を被覆した試料で超高真空測定セルを用いたガス平衡法（高温）である。

ⓒ ⓑの測定手段から得られた最も確からしい水素の拡散定数の値は，単純なアレニウス依存性を示さない。しかしこれは，本報告のChap. 2 に示したように，高温での鉄中の水素がDual Occupancy状態になることを考慮して導出した理論モデルとほぼ一致する。このモデルを基にした解析結果から，Tsites を経由しての水素の拡散のための活性化エネルギーとして 5.4 KJ /mol，高温でのそれとして 6.7 ～ 7.1 KJ /mol の値を得た。

ⓓ 拡散速度の測定法として今迄最も用いられている裸の金属を用いたPermeation 法，Desorption 法では，測定データの統計処理から，水素の拡散の為の見かけの活性化エネルギーの最確値として 8.5 KJ /mol を得た。この値は，バルク中の拡散のそれより大きく，測定の際に表面反応の影響を受けている可能性がある。解析の結果この活性化エネルギーの値は，酸素が吸着した裸の鉄表面での水素の脱離過程のそれに相当することが分った。表面反応の遅れを防止する為には，Pd のように化学的に貴で，水素の透過度が大きい金属の薄膜を皮覆した試料を用いるのが最適な手段である。しかし測定可能な温度域は限定される。

ⓔ Time－Lag などの簡便な過渡状態測定法は，拡散定数および溶解度が同時に測定出来，一見有効な手段のように思われるが，試料内の水素の拡散プロフィルが理想化した単一の拡散モデルの曲線と一致する試験条件でない限り，この手段により定常状態に相当する定量的な値を得ることができない。一般には，この手段が使われることが多いが，適用に際しては，試験法および理論解析上の検討が必要となる。

2） 鉄中の水素の拡散に及ぼす変形の影響

変形により生じた格子欠陥と水素との相互作用の研究は，実用材料における水素脆性の問題と関連して既に数多くの測定および理論的な解析がなされてきている。今迄提出されている報告を総合すると，加工材中の水素の拡散定数（D^{cw}）と完全結晶中のそれ（D^{p}）との比λは，次のいずれかの簡略化した式を用いて表現することができる。

$$\lambda = D^{cw} / D^{p} = [1 + K' \cdot \phi \cdot \exp(\Delta G^{*} / kT)]^{-1}$$

又は

$$\lambda = [1 + K' \cdot \phi \cdot \exp(\Delta G^{*} / kT)]^{-2}$$

ここでΔG^{*}は，本報告のChap 2に述べたように転位と水素との結合エネルギーに関係した定数，$K' \cdot \phi$は，欠陥濃度に関係した量である。これらの式に依れば，D^{cw}は，温度の低下と共に急速に低下し，低温では酸化物のそれよりも低いことにもなる。また常温付近で得られているデータとの適合性も良くない。この大きな原因は，前項に示したように表面状態の影響がある測定データを解析の対象として用いている事および水素の拡散に及ぼす転位の影響を単純化し過ぎている点にあると思われる。

水素の拡散に及ぼす加工歪の影響は，本報告Chap.2に示したように転位と水素との相互作用に置き換えて評価することができる。この報告では，水素の拡散に及ぼす転位の効果として，従来考えられている転位による水素のTrappingの負の効果の他に，今迄漠然と考えられていた転位芯の弾性応力場に沿った短範囲拡散（pipe diffusion）による正の効果を考慮し，新しい拡散のモデル式を提案した。この理論モデルを用いて表面状態の影響が少ない実測データを抽出して，これと理論モデルから算出した値との比較を行った。この結果，両者の適合性が非常によいことが分った。新しいモデル式および各パラメータは次の通りである。

$$\lambda = \gamma[(1 - \gamma) \cdot \sigma \cdot \exp(\sigma^{A} / kT) + \gamma]$$

$$\gamma = \theta^{L} / \theta_{I}^{cw} = [1 + \alpha \cdot \phi \cdot \exp(\Delta H^{*} / kT)]^{-1}$$

ここで$\sigma = 6.20 \times 10^{-3}$，$Q^{A} = 11.01$ KJ/mol，$\alpha\phi$およびΔH^{*}は，前項の値と同一である。また結晶粒界の影響についても粒界を転位の集積した界面と考える事により同モデル式で表現できることも明らかとなった。

3.2 General concepts

The preceding paper in this series [1] was concerned with the complications arising in the thermodynamic measurements in the H-Fe system due to both the non-regular mixing statistics and the effects of defects in the bulk and on the surface of the samples used to make measurements. It is not surprising that such a "sensitive" quantity as the temperature variation of the H-diffusivity should also reflect a strong dependence on experimental technique and sample preparation. A perusal of the large volume of H-diffusivity measurements [2-58] immediately reveals the existing extent of confusion and discrepancy. A discussion of the mass of data has been given by Völkl and Alefeld [44]. Whilst it is clear that the H-diffusivity should depend strongly upon deformation degree in cold-worked iron, there is also a large degree of discrepancy in the data obtained for well-annealed bcc iron [38-44], and the degree of discrepancy increases sharply with decreasing temperature. The measured diffusivities, taken as whole, begin a sharp drop at about 300K [38,44]. This is illustrated in fig. (1). A number of hypotheses have been suggested to account for this observation. We may list them briefly as follows:

(a) The presence of intrinsic trapping sites in the structure of well-annealed iron. Such models involve condensation of H-atoms under equilibrium conditions into tetrahedral sites (T-sites) [59] and other transition occupancy schemes involving more complex jumping mechanisms [60,61].

(b) Surface Effects. Sample pretreatment can lead to differing states of surface oxidation. This is often due to the presence of traces of water vapor in the experimental system [62]. Surface layers containing heavy concentrations of semi-microscopic voids and micro-cracks, formed by prior deformation, may not be removed by annealing [9,35,63].

(c) The presence of non-intrinsic defect sites in the bulk of the material. Such defects include sites related to impurity atoms, grain boundaries, and dislocations. They can all act as trapping centers for H-atoms at low temperatures [38,41,64-67].

How is the large band of scatter, and the decrease in D beginning at around room temperature as illustrated in Fig. (1), related to the factors (a), (b), and (c) outlined above? In reality there is a complicated combination of many factors involved. The "intrinsic" mechanisms (a) indeed predict a non-Arrhenius drop in the H-diffusivity D beginning at a critical temperature, but it cannot explain the large scatter band. Furthermore, it does not explain why such effects are not seen in other bcc metals. If H-H pairs on neighboring sites (T-T or O-O) (T=tetrahedral, O=octahedral) are invoked as an "intrinsic" H-trapping mcehanism, the same difficulties arise. Furthermore, there is no reason why such H-H-pairs will not be more prevalent in fcc metals [68].

Oxide film effects (b) will lead to a bend in the Arrhenius ln D vs. 1/T plot and its position (temperature) will depend on the experimental conditions (H_2O/H_2 ratio in the gas).

The situation in regard to surface and bulk defects not related to oxidation is more complex and has been discussed in Paper I of this series. Voids and microcracks cannot be removed by annealing, and, if present, will clearly lead to discrepancies. Other defects in the bulk may be partially removed by annealing but in any case they can be reduced to levels lower than $\sim 10^{-5}$ per atom which is required to explain the sudden drop in D at ~300°K (fig. (1)). However, an inappropriate post-annealing surface treatment such as those mechanical processes giving rise to Beilby layers or the rapid injection of H by electrochemical (charging) procedures can lead to defect-rich surface layers which can affect diffusion measurements even though the bulk material contains defect concentrations too low to cause anomalies to be observed.

Thus the problem is a complicated one and in this paper we will adopt the same procedure as in Paper I of this series [1] and discuss the diffusivity data in terms of the "best" data obtained selectively by rejecting data sets which are encumbered by the factors outlined under (b) and (c) above. The "selection rules" must give cognizance to the experimental method used in obtaining D-data, i.e. steady-state of transient techniques. For example, the surface reactions involving adsorption and desorption of H-atoms is very different when comparing H_2-gas equilibration and electrochemical techniques [69]. In the latter case the surface reaction may be controlled by changing the electrochemical potentials between the working electrode and the fiducial electrode. In contrast to this it is often not possible to maintain the surface state constant with time and/or H_2-pressure in permeation time-lag experiments.

The aim of the present report is to consider intrinsic and extrinsic sample-related effects in conjunction with the experimental techniques used and resolve the existing large volume of H-Fe kinetic data into an understandable scheme. Previous attempts have been made to simplify the situation by proposing "best" values for Q, the H-diffusion activation energy. Such values have been given by Ferro [70] (5.4 kJ/mol), Oriani [71] (7.95 kJ/mol) and by Völkl and Alefeld [44] who suggested two"best" Q-values according to the temperature range (4.18 kJ/mol at high temperatures and 10.05 kJ/mol at low temperatures).

In accord with the goal of this paper stated above, the first task to to take a close look at the diffusivities involved in the measurement techniques and attempt to draw up reasonable "selection rules".

3.3 H-DIFFUSIVITY IN WELL-ANNEALED IRON

3.3.1 Scatter in the measured data

A summary of representative measurement techniques for studying H-diffusivity in metals is given in Table I. The basic methods are split broadly into those depending on H_2-gas equilibration, electrochemical processes, and surface-independent techniques. It is clear that the surface-independent methods are superior in determining true bulk diffusivities, but, as shown in the last two columns of table I, they are limited by material and methodological (tracer handling) restrictions. Thus the bulk of the available data stems from H_2-gas equilibrium and electrochemical studies of both the transient and steady-state type.

Table II gives a summary of the results obtained using the equilibrium and electrochemical techniques. The table indicates sample purity and surface pretreatment (when given) and the temperature range spanned. Each data set is assumed individually to conform to the Arrhenius relation

$$D = D_o \exp(-Q/kT) \qquad (1)$$

the the best values of D_o and Q obtained by least-squares regressions are also given. The large degree of inconsistency can be seen at a glance. The data of table II are given in fig. (2). The representative lines in fig. (2), delineated by the symbol at the maximum and minimum measuring temperatures, are constructed from the Q and D_o values given in table II. The lines are identified by the symbols shown in the last column of table II which indicates the author reference and measuring method class. Now, although it cannot be portrayed on fig. (2) for obvious reasons of clarity, almost all of the 36 individual data sets of fig. (2) and table II are consistent with equ (1) within their own temperature range, and often exhibit only a small degree of scatter. It is noteworthy that these three sets of H_2-gas

equilibration data using Pd-coated samples (T range ~ 325-823K) show mutually consistent values of both Q and D_o. This is strong evidence that metallurgical factors such as grain size or impurity levels do not cause data discrepancies above 350K when the surface condition does not affect the measurements. The Pd-coating in the H_2-gas equilibration method [1-3] was developed for the specific purpose of accelerating the adsorption or desorption process. Its application is limited to temperatures at which there is a low interdiffusion coefficient between the coating and the matrix material. In the case of electrochemical methods, the Pd or Ni coating is used to diminish corrosion at the H-output side under the anodic potential.

Let us now attempt to correlate the apparent diffusivities to the technique used to measure them using the information contained in table II and fig. (2).

3.3.2 The Relationship Between Apparent Diffusivity and Measurement Technique

The data assembled in table II have been used to construct the histogram shown in fig. (3). The histogram was constructed by assuming that each data set has standard deviation of $\pm$2.1 kJ/mol ($\pm$0.5 kcal/mol) in the value of Q. If the individual experimental techniques were truly equivalent, the statistical distribution of Q-values would be independent of the actual technique used. The histogram clearly shows that this is not the case. Not only does the H_2-gas equilibration method show much scatter amongst the individual Q-values, below 470K, but the trend of values is markedly dependent upon the actual method (i.e. steady-state or transient). Thus the differing measurement techniques are clearly not equivalent. The data distribution having the lowest activation energy is found using Pd-coated specimens and UHV techniques in the gas equilibration method and the electrochemical method.

If we consider that the minimum D-values represent the true bulk material diffusivity, then these latter techniques are capable of providing reliable

data. It has often been considered that the H_2-gas equilibration method using uncoated specimens was appropriate at high temperatures [38,41], but, as Fig. (3) shows, large mutual discrepancies occur above 470 K.

This conclusion may be confirmed by calculating the probability P_G of occurrance of a datum (in this case-ln D) at a given temperature assuming a Guassian distribution [72] in the form,

$$P_G = \frac{1}{\sigma \sqrt{2\pi}} \exp \left[-\frac{1}{2} \left(\frac{x-\mu}{\sigma} \right)^2 \right] \tag{2}$$

where μ , the mean value of the datum ($x = -\ln D$), is given by

$$\mu = \frac{1}{N} \sum_{i-1}^{n} f_i \, x_i \tag{3}$$

and the quantity x is taken in n increments of Δx_i such that the total number of data N is,

$$N = \int_o^{\infty} (\Delta x_i \, f_i) d(\Delta x) \tag{4}$$

Equation (4) serves to define f_i. The quantity σ is the standard deviation, given by [72],

$$\sigma^2 = \frac{1}{(N-1)} \sum_{i=0}^{n} f_i \, (x_i - \mu)^2 \tag{5}$$

The relation (2) has been used to calculate P_G at a series of temperatures using data sets split into groups according to the various measuring techniques. The results are shown for the temperature T=248K in fig (4) in comparison with the corresponding histograms. All the original data in table II were used. The peak value of ln D taken from the histograms is labeled μ_m. This clearly does not coincide with the probability peal $P_G(P)$ calculated from equ.(2) using

all the data (dashed line in upper part of fig. (4)). This mean calculated value is μ_p. The data points in the range $0 \leq -\ln D \leq \mu_m$ i.e. to the left of μ_m in the diagrams have been fitted to a Guassian distribution $P_G(M)$ and this is shown by the solid line in Fig. (4). The coincidence between $P_G(M)$ and $P_G(P)$ and the lower extent of scatter for the electrochemical determinations in comparison with the equilibration methods is clearly seen (lower section of fig (4)).

The calculations upon which fig. (4) are based were repeated for several temperatures spanned by the available data ensuing from the H_2-gas equilibration measurements of table II. The most probable values μ_m of $x = -\ln D$, calculated from the peak value of $P_G(M)$, (symbol ●) and the mean value of μ_p of ln D obtained from the peak values of the calculated $P_G(P)$ (equ. (4)) are given in an Arrhenius plot vs. reciprocal temperature in fig. (5). The thick upper solid line represents μ_m (symbol ●) and the lower dashed line is μ_p (symbol ○). The error bar ranges ($\pm \sigma_M$ or σ_p) are given by the corresponding dashed or (thin) solid lines. The large values of $\sigma_{M,P}$ at low temperatures are clearly seen. The most probable values (●) taken within this group of data sets, i.e. for this experimental method, show adherence to the linear Arrhenius relationship. The representational equation corrsponding to the μ_m values of fig. (5) is,

$$D = 6.70 \times 10^{-8} \exp(-Q/RT)\ m^2/sec \qquad (6)$$

where Q is 8.37 kJ/mol.

Now the analysis just presented may be reproduced for each class of experimental measuring conditions and techniques. This analysis has been performed and the results are presented in fig. (6) and table III. This table gives the statistical analysis results for the experiment groups which

have been classified as A (H_2-equilibrium, Pd-coated UHV), B (electrochemical), C (H_2-equilibrium, no coating), and D (samples contained surface trapping sites due to either inappropriate pretreatment or experimental procedures). The determination of the "best" values of Q and D_o and their concomitant σ_m-values leads to the bounding lines and corresponding, partly overlapping regions, A,B,C and D in Fig.(6). The large region D in fig (6) corresponding to high degrees of scatter and large values of Q results from transient-type (time-lag) H_2-gas equilibration methods. The region C corresponds to steady-state H_2-gas equilibration techniques. The regions A and B include data obtained without interfering surface effects playing a role. The actual temperature range spanned by the individual $\pm\sigma_m$ envelopes is indicated by the solid lines and the dashed lines are extrapolations.

The next section of this report will be devoted to a discussion of the diffusion data corresponding to the several areas in fig. (6).

3.3.3 Analysis of Diffusion Data

a) Regions A and B (fig (6))

The data of regions A and B (fig. (6)) correspond to the diffusion of H through the bcc Fe lattice when the data are not encumbered by the presence of spurious effects due to the nature of the sample surface. The data of regions A and B are shown in a magnified form in fig. (7). The higher temperature region A, stemming from three sets of experiments [2,3,4] using the H_2-equilibration method with Pd-coated specimens and UHV apparatus clearly have much more scatter than the 20 sets of determinations taken from electrochemical data at the lower temperatures (region B). The average values of the region A data (---) are somewhat larger than those of the electrochemical data extrapolated into region A and the corresponding Q-values are somewhat different (i.e. 6.69 - 7.12 kJ/mol (A) and 5.69 kJ/mol (B), see table III). Now although

the data input level in region A is relatively sparse, and $\pm\sigma$ correspondingly greater, the question should be posed as to whether or not this difference represents the "true" behavior of the H-Fe system or is it yet another artifact related to differences in experimental technique.

In paper I of this series [1] the thermodynamic properties of H dissolved in well-annealed iron were explained by the dual occupancy model in which the tetrahedral (T) sites are more stable at low temperatures and the octahedral (O) sites become occupied with increasing fraction of H-atoms as the temperature increases. The change is the partial enthalpy and non-configurational entropy accompanying a T → O transfer of an H-atom were found to be $\Delta\bar{H} = -22.56$ kJ/mol and $\Delta\bar{S} = -6.0$ k. These values are consistent with the thermodynamic behavior of the system. If this concept is valid, dual occupancy must also manifest itself in the kinetic behavior of the system. In the simple classical approach, normal Arrhenius diffusion corresponding to T→T jumps would be expected. At higher temperatures atoms jumping from O-sites will make a contribution to the diffusion flux. Now an atom instantaneously in an O-site can make O-T-O jumps in the bcc lattice. Jumps between T sites may take either of two paths, i.e. T-T, and T-O-T. In a small volume element in quasi-static equilibrium with its surrounding crystal, the frequencies of such jumps must, by the principle of microscopic reversibility, be such as to conserve the equilibrium numbers of H-atoms at T and O sites. This means that the diffusivity D^M can be written, with obvious notation in the form

$$D^M = f\,\Phi\,D^{T-T} + (1-f)\,\Phi\,D^{T-O-T} + (1-\Phi)\,D^{O-T-O} \qquad (7)$$

where Φ is the fraction of H-atoms instantaneously on T-sites at a given temperature and $(1-\Phi)$ the corresponding fraction of O-sites. The fraction of H-atoms instantaneously hopping by the T-T direct mechanism is f, and that undertaking T-O-T jumps is (1-f). Now the linearity of the Arrhenius plot

for region B and the fact that the T-O-T path length is 41% longer than the T-T path length (see fig. 8) indicates that $f \approx 1$ is a reasonable approximation so that,

$$D^{M} = \Phi\, D^{T-T} + (1 - \Phi)\, D^{O-T-O} \qquad (8)$$

Now [73] the value of Φ is given by

$$\Phi = [\, \frac{1}{2}\; e^{\Delta\bar{H}/kT}\; e^{-\Delta\bar{S}/k} + 1]^{-1} \qquad (9)$$

The center (thicker) line in Fig. (7) is constructed from the values of D^{T-T} and D^{O-T-O} taken from table III and equ. (8) using the values of $\Delta\bar{H}$ and $\Delta\bar{S}$ taken from the analysis of the thermodynamic data (i.e. $\Delta\bar{H}$ = - 22.56 kJ/mol, $\Delta\bar{S}$ = -6.0 k). It is clear from fig. (7) that the kinetic data are entirely compatible with the interpretation of the thermodynamic data in terms of the dual occupancy model. It is also clear that more data are required in region A. In this context "region A" does not just mean this temperature range, but implies that a surface-independent method, or a method free of spurious surface effects be used.

It is clear that the H-atoms occupy the T-sites preferentially at low temperatures and are thus located in the symmetrical crystal field [74]. However, the real situation may in fact be more complex and models have been discussed in which the H atoms in bcc metals are not considered as being located in a classical manner as a bound oscillator at a point (1T in fig. (8)), but rather occupy "tunnel split states"[61] in which the H-wave function spreads into neighboring dissimilar states or is "smeared" in 4T or 6T rings [60,61] (see fig. (8)). The long-distance distribution of the H wave function along such T-site configurations has been discussed by Richie et. al [92]. However, the energy differences between such configurations are small [60,61,75] (1-5 meV) and it is most probable that in Fe the difference between the A and

and B regions, which requires further experimental investigation, is due to the transition between a T (or T-group) configuration, and the O-configuration. The classical [76] value of the diffusivity ratio between H and D in bcc iron, i.e. $(M(D)/M(H))^{1/2} = 1.41$ is not observed. Its value is about 2 at high temperatures and ~1.2 at low temperatures. Thus the problem of the real mechanism of H-diffusion in the bcc Fe lattice is complicated by non-classical effects [3,77] and a final solution must involve quantum mechanical modification to the classical transition rate model [78] and a consideration of tunneling from one interstitial configuration state to another [77].

b) Region C (fig. 6)

The data of region C were obtained predominantly by using the steady-state H_2-gas equilibration method without a protective surface coating on the iron membrane. As the data analyses show (see Tables I and II and fig. (6)), the measured diffusivities, although smaller than region A and B, are still compatible with the Arrhenius representation and a larger activation energy. This difference is due to effects connected with the sample surfaces. The surface effects may be divided into two catgeories, namely the dissociation of hydrogen gas at the input side and the hydrogen desorption-recombination at the membrane output side. Since, however the chemical potential of H at the input surface is usually many orders of magnitude higher than that at the outlet surface, the interfering effects are usually restricted to the latter surface. In the experimental procedures involving Pd-coating, usually only the outlet surface is coated.

The release rate F of H on the outlet side of the sheet of semi-finite thickness if given by [79,80]

$$F = -D \left(\frac{\partial c}{\partial x} \right)_{x=0} = -\alpha C_S$$

where C_s is the H concentration at the output surface and α is the surface reaction rate at time t. If F_o is the gas release rate at the output surface at time t=0 the use of Fick's second law leads to the well-known relation [79],

$$\frac{F}{F_o} = \exp \left\{ q \ [1 - \mathrm{erf} q^{1/2}] \right\} \tag{10}$$

where $q = (\alpha^2/D)^t$ (11)

This relationship is shown in representative form in fig (9) for both steady-state evaluation methods (fig. (9) I) with and without a surface effect and for time-lag evaluation methods (fig. (9) II) for differing times t_1 and t_2. In these diagrams C_S^o is the steady-state value of the outlet surface concentration. For a sheet of finite thickness l the time variation of M, the volume of H_2 liberated (or pressure increase) at the output side is related to time as shown in fig. (10). The slopes m_i correspond to the time periods t_i. Now on a real surface α is a function of H concentration and time. The form of F in terms of the "true" bulk diffusion coefficient have been derived by Crank [79] for various representative surface reactions. The results have been collected in a condensed form in table IV. This table also contains the nomenclature used. Note that k_1 is a function of time. Now the adherence of the data of region C to an Arrhenius representation implies that the surface effect is a rapid and irreversible trapping of H at the surface. This surface reaction corresponds to the apparent steady-state diffusivity $(Dk_1)^{1/2}$ (last column of table IV). Thus if the surface rate constant can be written $\kappa \exp(-Q_K/kT)$, where κ is the appropriate pre-exponential factor and Q_k the activation energy for the surface reaction, then the apparent diffusivity D^{app} is

$$D^{app} = [\kappa D_o e^{-Q/kT} e^{-Q_k/kT}]^{1/2}$$

so that, with obvious notation, the "apparent" activation energy is given by,

$$Q_{app} = \frac{1}{2} [Q + Q_k]$$

Using the value Q_{app} = 8.37 kJ/mol and the true bulk activation energy Q = [5.44 - 7.21] kJ/mol (see table III), yields the value Q_k = 9.6 - 11.3 kJ/mol. Now the possible surface reactions including desorption on the clean metal surface, surface diffusion of H, the recombination of H on many ceramic, oxide and graphite layers, and desorption of H from a surface heavily contaminated with adsorbed oxygen have all been studied experimentally [79-83]. Except for the latter reaction, the activation energies are all 1-0.5 orders of magnitude larger than the Q_k-value deduced above [~10 kJ/mol]. The activation energy for H-desorbtion from the oxygen-contaminated layer is [6.3 - 12.6 kJ/mol] [80-83]. Thus the evidence is strong that this is indeed the rate-limiting mechanism and the surface reaction is the first-order desorption of H from an oxygen-adsorbed surface. UHV experiments [84] show that pre-annealing at moderate temperatures will result in a layer of adsorbed oxygen. In general the experimental systems used in permeability time-lag experiments in region C maintain a pressure in the region of 10^{-3} Pa on the outlet side of the membrane, or use an inert carrier gas with sufficient impurities to cause contamination. It is difficult to remove surface contamination even in UHV work and Pd-coating would seem to be the best solution to the problem.

C) Region D (fig. 6)

As shown in the previous section (II) of this report, a reasonable statistical data analysis indicates that the large spread of measured data falling into region D is not due to "normal experimental error". The much lower diffusivities found in this region indicate that the observed decrease in apparent mobility is not simply due to a surface-contamination

effect as found for region C, but rather to a combination of trapping effects related to trapping defects generated during sample pretreatment. The existence of trapping sites in the bulk material related to lattice defects (dislocations) is undoubtedly a causative mechanism and their effect will be discussed at length in the next section of this report. Theoretical treatments of H-diffusivity in bcc iron based upon H-trap interactions are well-known. However, the atomic concentration [defects per Fe-atom] required to explain the sharp drop in D-values in region D is the order of 10^{-5} [38]. Such high defect concentrations are not present in well-annealed iron. Thus other mechanisms must be invoked. One such possibility is the presence of the Beilby layer formed by the mechanical abrasion of the iron membrane. Such layers [1] contain high defect concentrations and cannot be completely removed by annealing. If the membrane used in the diffusivity experiments was thin, the defect-rich surface layers can cause a significant reduction in H flow rate through the sample. If the solubilities in the bulk and defect layers are θ^b and θ^d, the apparent diffusivity D^{app} can be written [85]

$$D^{app} = \frac{1}{\theta^{app}} \left[\frac{\gamma_s}{D^d \theta^d} + \frac{1-\gamma_s}{D^b \theta^b} \right]^{-1} \tag{11}$$

where

$$\theta^{app} = \gamma_s \theta^d + (1 - \gamma_s) \theta^b \tag{12}$$

where D^b and D^d are the bulk material and defect layer diffusivities and γ_s is the thickness of the defect layer divided by that of the bulk material. Thus D^{app} can be decreased by low values of D^d coupled to large γ_s-ratios. It is not surprising that the measurements exhibit much scatter from data set to data set. Furthermore there is always the possibility that the dislocation density has not been reduced to the minimum value corresponding to "well-annealed iron" and trapping at dislocation-related sites can be important in some of the

data sets in region D. As pointed out previously [38], trapping effects in Fe are prone to be observable since the "normal" activation energy is small [Q ≈ 4-8 kJ/mol] and what is important is not just the depth of trapping sites, but their depth relative to that ot "normal" sites. In nickel, where Q is about five times larger than that for Fe, the same concentration of defects would cause an observable reduction in H-mobility only at much lower temperatures than in iron.

d) Summary

In order to summarize the previous discussions of the H-diffusivity in terms of splitting the observed phenomena into the regions A, B, C, and D of Fig. (6), let us reiterate the causes of the apparent confusion in terms of the characteristics of the metal iron.

(a) In the bcc metals in general [73] and in bcc Fe in particular, the activation energy for H-diffusion is small, about one tenth the value for fcc metals. Thus at low temepratures the H-diffusion rate in iron is faster than surface reaction rates with contaminants. This is normally not true in fcc metals.

(b) The H-solubility in bcc iron is small (10^{-6}-10^{-8} atom ratio below 300K) and thus at such low temperatures a significant fraction of the total H-concentration can be trapped, especially in defect-rich surface layers. Because of (a) above, even relatively shallow trapping sites will cause a more significant reduction in the observed mobility of hydrogen [38] than would be the case for metals exhibiting a larger activation energy for "normal" site jumps.

(c) Iron is a chemically active element and it is relatively difficult to prevent surface contamination and this problem requires careful attention in respect to H-diffusivity measurements. Electrochemical

polishing and surface coating with a noble metal having a high hydrogen diffusivity and solubility are appropriate surface treatments. However, at high temperatures the coat-bulk interdiffusion provides a limitation so that coated specimens can only be used in a fairly restricted temperatures range.

3.4 HYDROGEN DIFFUSIVITY IN DEFORMED IRON

Let us now attack the problem of the diffusivity of hydrogen in deformed (cold-worked) iron. Not only is this problem one of great technological importance in regard to such effects as hydrogen embrittlement, but has also played an important role in the development of the theories of the trapping of interstitial atoms at defect sites in metal lattices. It has been the subject of numerous investigations [86,87,89]. The analysis of theoretical models using experimental diffusion data obtained from deformed samples is rendered problematical, in the same way as the evaluation of thermodynamic models [1], by the fact that the comparison data must be carefully selected so as to exclude such data which are encumbered with spurious effects. In the present section of this report only diffusivities obtained using the electrochemical method will be employed [29,32,88]. The diffusivities in the non-deformed state (D^P) are taken from a single crystal work of Yamakawa et. al.[29] and for the deformed state (D^d), the data of Yamakawa et. al [88] obtained on material deformed in the range 5.8 - 31% are employed.

Now several diffusion models have been proposed [38,41,64,65] to account for the motion of an interstitial atom in a crystal containing trapping sites. Their results may be represented in summary by the relations,

$$\frac{D^d}{D^P} = \lambda = [1 + \kappa'\phi\exp\left(\frac{\Delta G^*}{kT}\right)]^{-1} \quad \text{(refs. 41,64,65)} \tag{13}$$

$$\lambda = [1 + \kappa'\phi\exp\left(\frac{\Delta G^*}{kT}\right)]^{-2} \quad \text{(ref. 38)} \tag{14}$$

where ΔG^* is the depth of the trapping sites with respect to normal sites, κ' is a constant and ϕ is the number of defect sites per metal atom. The reasons for the difference in form between expressions (13) and (14) have been discussed recently [90].

Now expressions (13) and (14) are based upon statistical models in which two energy levels, i.e. "normal" and "trapping" levels, are considered. However, in reality, a dislocation is associated with an elastic field which interacts with dissolved H-atoms. Thus, especially when the dislocation density is high, several energy levels are involved. An excellent recent discussion of the nature of this interaction has been given by Hirth and Carnahan [91]. However, in order to set up a viable statistical model, it is necessary to restrict the number of energy levels otherwise the calculated solubility or diffusivity expressions will contain too many unknowns to enable a comparison with experimental data to be effected. Thus in the present paper we will adhere to the two-energy-level approach, but attempt to account for the dislocation stress field by a simple purturbation of the saddle point energies for H-atom jumps involving sites close to dislocation trapping sites. This simple concept is illustrated by the energy level scheme given in Fig.(11).

The upper diagram of Fig. (11) depicts thermally activated hopping over the potential barriers around T-sites (low temperatures). The activation energy is Q^P (P="perfect"). The center diagram represents a H-atom in a dislocation-related trap site. The activation energy required to jump from such a site is Q^t. Now, in the simple model presented here, the effect of the dislocation stress field is to lower the energy barrier for jumps from

sites neighboring trapping sites into the traps themselves but not to purturb the energy minima of sites which are not trapping sites. This state is represented in the center of Fig. (11). It is then assumed that hops occur with such a frequency that, in a given volume element, the equilibrium values of the numbers of H-atoms on the two energetically distinct sites are maintained. As shown previously [1], the concentration of H-atoms in the deformed crystal, θ_i^{CW}, is apportioned between the trapping sites (B) and the "normal" sites (L) such that

$$\theta_i^{CW} = \theta_L + \theta_B \tag{15}$$

and $$\theta_i^{CW} = \theta_L \left(1 + \alpha\phi \exp \frac{\Delta H^*}{kT}\right) \tag{16}$$

where ΔH^* is the depth of trapping sites, $\alpha = \exp(-\Delta S^*/k)$ the corresponding entropy term and ϕ is the density of trapping sites. Now the previous analysis of the solubility of H in cold-worked iron in terms of the distribution (16) showed that $\alpha\phi = 2.04 \times 10^{-20}\ \phi'$, where ϕ' is the dislocation density in the cold-worked (CW) iron per m^2, and the trapping depth is $\Delta H^* = 33.9$ kJ/mol.

Now in keeping with equ. (7) let us write the diffusivity D^{CW} in the deformed material in terms of the fractions of H-atoms in the two distinct energy configurations and their concomitant diffusivities, i.e.

$$D^{CW} = \frac{\theta_L}{\theta_i^{CW}} D^L + \frac{\theta_B}{\theta_i^{CW}} D^B \tag{17}$$

or $$D^{CW} = D^L - \left(\frac{\theta_B}{\theta_i^{CW}}\right) [D^L - D^B] \tag{18}$$

where equ. (15) has been used.

Now in accord with fig. (11) the value of D^L can be written in the form,

$$D^L = D^P [\sigma \exp (Q_A/kT)]\ \delta + D^P (1-\delta) \tag{19}$$

This equation is to be interpreted in a semi-quantitative way by reference to fig. (11). The upper part of fig. (11) depicts diffusion by classical thermally activated hopping over the potential barrier between adjacent T-sites. This is the (low temperature) hopping mechanism for H-atoms in L-sites at large distances from the dislocation lines. The fraction of atoms instantaneously on such sites and hopping by this mechanism is $(1-\delta)$. A fraction δ of the H-atoms on N sites is in close proximity to the dislocation and, in this simplified concept, the stress field has the effect of perturbing the potential barrier for hops into a defect site (center diagram, fig. (11)) and furthermore the jumps into adjacent sites in a direction parallel to the dislocation line are also reduced in the same manner (lowest diagram fig. (11)). This mechanism is effectively a "pipe" diffusion along dislocation lines. The term $\sigma \exp (Q_A/kT)$ in equ. (19), where $Q_A > 0$, represents the enhancement in the mobility of H-atoms due to the reduced potential barriers as discussed. The energy Q_A and the preexponential factor σ are to be understood in a qualitative sense only since the treatment of "normal" T-T hops let alone hopping by the tunnel states (fig. (11)), in classical terms is questionable.

Now combining equs (18) and (19) gives the following expression for the diffusivity ratio $\lambda = D^{CW}/D^{P}$,

$$\lambda = \frac{\delta \sigma \exp (Q^A/kT) + (1-\delta)}{1 + \alpha \phi \exp (\Delta H^*/kT)} + \frac{\theta_B}{\theta_i^{CW}} \cdot \frac{D^B}{D^P} \qquad (20)$$

Now $\theta^B/\theta_i^{CW} < 1$ and since $D^B/D^P << 1$ the second term in equ. (20) is negligible. In fact D^B/D^P is of the order $\exp (-\Delta H^*/kT)$. At 300 K, using the value $\Delta H^* = 33.9$ kJ/mol deduced from the thermodynamic behavior or the Fe-H system [1], $D^B/D^P \simeq 10^{-6}$.*

* Footnote: The lowest measured values of λ are about 10^{-3}.

Now the value of the factor $\sigma \exp (Q^A/kT)$ may be deduced from the diffusivity measurements since if the temperature is sufficiently low and the trap site density sufficiently large then $\delta \simeq 1$ and, from equ. (20),

$$\lambda = \frac{\sigma \exp (Q^A/kT)}{1 + \alpha \phi \exp (\Delta H^*/kT)} . \qquad (21)$$

Thus a plot of $\ln [\lambda (1 + \alpha\phi \exp (\Delta H^*/kT)]$ vs. $1/T$ will have a slope of Q^A/k and an intercept given by $\ln \sigma$ as $T \to 0$. This evaluation has been performed using the D^P-value for Fe single crystals [29] and D^{CW} measurements on deformed iron using the electrochemical method [88]. The values of $\alpha\phi = 4.31 \times 10^{-20} \times \phi'$, where ϕ' is the measured dislocation density [88] and $\Delta H^* = 33.9$ kJ/mol are taken from the previous thermodynamic analysis [1]. The results are shown in Fig. (12). The data for each deformation degree (ϕ'-value) were plotted as described above and the data subject to a least-squares regression to obtain the best values of α and Q^A. As can be seen in fig. (12) the values of α and Q^A become constant as ϕ' exceeds $\sim 3 \times 10^{14}$ m^{-2}. The corresponding values of σ and Q^A are $\sigma = 6.20 \times 10^{-3}$ and $Q^A = 11.01$ kJ/mol. The comparison between the measured values of λ and those predicted from equ. (20) requires, of course, the estimation of δ. This is a complex problem and in this report we shall make the simple assumption that $\delta \simeq \theta_B/\theta_i^{CW}$, i.e. that the ratio of H-atoms in L-sites instantaneously undergoing jumps in the direction of the reduced energy barrier to total number of H-atoms in L-sites is approximately equal to the fraction of H-atoms in traps. Although this is only an approximation it will certainly reflect the correct behavior as ϕ' increases since, as the trap density increases, both θ_B and δ must increase. Using the abbreviation $\gamma = \theta^L/\theta_i^{CW} = [1 + \alpha\phi \exp(\Delta H^*/kT)]^{-1}$ and equ. (20) (without the last term), gives finally,

$$\lambda = \gamma [(1 - \gamma) \sigma \exp (Q^A/kT) + \gamma] . \qquad (21)$$

A comparison between the measured [29,88] values of λ and those calculated from equ. (21) is given in fig. (13) in which the calculated λ - values (solid lines) are compared with the measured diffusivity ratios. Each symbol corresponds to a different dislocation density. The satisfactory agreement between experiment is apparent.

Now the question of the influence of grain boundaries acting as trapping sites for H in iron has also been discussed frequently. Recent work by Hagi et. al [32] provides excellent data for the evaluation of this phenomenon. In this work the H-diffusivity in an Fe sample deformed 10%, a non-deformed polycrystalline Fe with a grain size of 17 μm, and a single crystal Fe was measured at a series of temperatures below room temperature (289-244 K). The diffusivity ratios λ have been calculated from these results using the single crystal data in their experiments for D^P. The results are shown in Fig. (14). No dislocation densities were measured in this work so the measured λ-values were fitted to equ (21) using a series of successive ϕ'-values. It can be seen that, for the cold-deformed sample, the model equation is consistent with the measurements for a dislocation density of $\phi' = 2.5 \times 10^{14}\ m^{-2}$. This is a reasonable result for 10%-deformed material.

Now the same equation (i.e. (21)) is used to calculate λ for the non-deformed polycrystalline sample (uppermost data set of fig. (14)). The same value of ΔH^* was used (33.1 kJ/mol). It can be seen that the rather limited data are consistent with the calculated λ-values for a "dislocation density" of $\phi' = 2 \times 10^{12}\ m^{-2}$. However (see equ. (16)) this means that the density of trapping sites is $\phi = 2.04 \times 10^{-20}\ \phi'/\alpha = 4 \times 10^{-8}$. This is a reasonable result for a material with a grain size of 17 μm. An estimation of ϕ based upon identical grains separated by grain boundaries having the maximum dislocation density (i.e. just before "rupture") gives $\phi = 2.24 \times 10^{-7}$.

The constant $\alpha = \exp(-\Delta S^*/k)$ is not expected to depart significantly from unity. The implicit assumption that trapping sites related to grain boundaries have the same depth as those related to dislocations is, of course, quite arbitrary.

Let us compare the predictions of the present model, i.e. equ. (21) with those of equations (13) and (14). Using a defect concentration corresponding to $\phi' = 1.5 \times 10^{15}\ m^{-2}$ and writing $\kappa\phi\exp(\Delta G^*)$ in equations (14) and (15) as $\alpha\phi \exp(\Delta H^*/kT)$, the values of λ for $\Delta H^* = 33.9$ kJ/mol can be calculated from equs. (13), (14), and (21). The results are shown in fig. (15). The decrease in λ with decreasing temperature is not so sharp in the present model as that predicted by equs (13) and (14) for a given trap depth and concentration. However, as outlined in depth in previous sections of this paper, much of the sharp decrease in D in the case of both "well-annealed" and deformed iron is due to spurious surface effects.

This report has presented an approach to the problem of the diffusivity of H in deformed Fe which represents a much simplified and indeed semi-quantitative treatment of a complex process. The degree of agreement between the predictions of the model and actual experimental data however gives credence to the assumption that the localized distribution of H atoms in close proximity to dislocation trapping sites plays an important role in the diffusion of an interstitial species in deformed metals. There is effectively a "pipe diffusion" component which acts in an opposite sense to the retardation of mobility due to the trapping sites per se. This is why the λ-values calculated from equ. (21) do not decrease as sharply with decreasing temperature as do the values consistent with equs (13)and (14) (see fig. (15)). It is however well to point out that all of these models represent great simplifications to an intrinsically complex problem since even in the case of H-diffusion in defect-free iron the effects of tunneling, "ring" diffusion, and "small polaron behavior" have yet to be worked out.

3.5 CONCLUSIONS

The consideratons presented in this paper may be summarized in the following way:

(A) Hydrogen diffusion in well-annealed iron.

(A-1) The large degree of mutual disagreement and departure from Arrhenius behavior exhibited by the large volume of diffusion data is largely a function of spurious surface effects and does not represent an intrinsic feature of the H-Fe system.

(A-2) At low temperatures H diffusion data obtained using electrochemical techniques adhere to the Arrhenius relation and exhibit the low activation energy of 5.4 kJ/mol. This energy is taken to represent the diffusion energy barrier between adjacent tetrahedral sites.

(A-3) Hydrogen diffusion measurements, free of spurious surface effects, and carried out at higher temperatures also show linear Arrhenius plots but consistent with a slightly higher activation energy of 6.7 -7.1 kJ/mol.

(A-4) The difference in activation energy as under (A2) and (A3) is consistent with the increasing occupation of octahedral interstitial sites as the temperature is increased.

(A-5) The apparent activation energies of ~8.5 kJ/mol found using H_2-gas equilibration techniques can be interpreted in terms of the reaction rate for the desorption-recombination of H on the oxygen-contaminated outlet side of the membranes used in the diffusivity determinations.

(A-6) The apparent diffusivity obtained using samples with unappropriate surface conditions is a function of the experimental technique employed in respect to steady state or transient methods.

3.6 REFERENCES

[1] K. Kiuchi and R. B. McLellan. Submitted to Acta Metall.

[2] R. F. Miller, J. B. Hudson and G. S, Ansell. Met. Trans. A 6a 117 (1975).

[3] H. G. Nelson and J. E. Stein. NASA Tn D-7265 (1972).

[4] N. R. Quick and H. H. Johnson. Acta Metall. 26 903 (1978).

[5] C. Sykes, H. H. Buron and C. C. Gegg. J. Iron Steel Inst., 156 155 (1947).

[6] H. Schenk and H. Taxhet. Arch. Eisenhüttenwes. 30 661(1959)

[7] W. Geller and T. H. Sun. Arch. Eisenhüttenwes. 21 423 (1950).

[8] E. Domke. Thesis Univ. Münster, Germany (1971).

[9] H. J. Koenig and K. W. Lange. Arch Eisenhüttenwes. 46 669 (1975).

[10] H. Maas. Thesis Univ. Münster, Germany (1971).

[11] F. E. Jesnitzer and H. Hieber. Arch. Eisenhüttenwes. 40 73 (1969).

[12] T. Heumann and D. Primas. Z.Naturforsch. 21a 260 (1966).

[13] D. C. Carmichael, J. R. Hornaday, A. E. Morris, and N. A. Parlee. Trans.Met. Soc. AIME 218 826 (1960).

[14] W. Eichennauer, H. Künzig and A. Pebler. Z. Matallk. 49 220 (1958).

[15] T. M. Stross and F. C. Tomkins. J. Chem. Soc. 159 230 (1956).

[16] E. W. Johnson and M. L. Hill. Trans. Met. Soc. AIME 28 1104 (1960).

[17] H. Zitter and H. Krainer. Arch. Eisenhüttenwes. 29 4C1 (1958).

[18] R. W. Lee, D. E. Swets, and R. C. Frank. Me.. Sci. Rev. Met. 58 36 (1961).

[19] G. M. Evans and E. C. Rollanson. J. Iron Steel Inst. 207 1484 (1969).

[20] W. L. Bryan and B. F. Dodge. AIChEJ 9 223 (1963).

[21] J. Y. Choi. Met. Trans. 1 911 (1970).

[22] R. Wagner and R. Sizmann. Z. Angew Phys. 18 193 (1964).

[23] W. Raczynski and S. Stelmach. Bull. Acad. Pol. Sci. Ser. Sci Chim, 9 633 (1961).

[24] S. Wach and A. P. Miodownik. Corr. Sci. 6 271 (1966).

[25] J. Chene, J. Galland and P. Azou. Hydrogen Met. Proc. Int. Congr. 2nd 1a3 (1977) Pergamon. Oxford.

[26] B. K. Reiermann. Thesis Thech. Univ. Berlin D83, Germany (1970).

[27] R. M. Barrer. Trans. Faraday. Soc. 36 1235 (1940).

[28] R. C. Frank, D. E. Swets and D. L. Fry. J. Appl. Phys. 29 892 (1958).

[29] Y. Yamakawa, T. Tsuruta and Y. Yoshizawa. J. Boshoku Gijutsu 30 443 (1981).

[30] W. Beck, J.O'M Bockris, J. McBreen and L. Naris. Proc. Roy. Soc. Ser. A 290 220 (1966).

[31] J. McBreen. Ph.D. Thesis Univ. Pennsylvania (1971).

[32] H. Hagi, Y. Hayashi and N. Ohtani. Trans. JIM 20 349 (1979).

[33] W. Raczynoki. Phys. Status Solidi A 48 K27 (1978).

[34] S. Asano, K. Hara, Y. Nakai and N. Ohtani. J. Japan Inst. Metals 38 626 (1974).

[35] P. K. Subramanyan. Ph. D. Thesis Univ. Pennsylvania (1971).

[36] A. J. Kumnick and H. H. Johnson. Met. Trans. 5 1199 (1974).

[37] A. K. Mindyuk and E. I. Svist. Fiz-Khim Mekh. Mater. 9 36 (1973).

[38] R. B. McLellan. Acta Metall. 27 1655 (1979).

[39] O. D. Gonzalez. Trans. AIME 245 607 (1969).

[40] V. P. Alikin. Isv. Estestvennonauchn. Inst. pri Permsk Univ 14 19 (1960).

[41] R. A. Oriani. Acta Metall. 18 147 (1970).

[42] O. D. Gonzalez. Trans. AIME 239 1041 (1967).

[43] T. P. Radhakrishman and L. L. Shreir. Electrochim Acta 12 889 (1967).

[44] J. Völkl and G. Alefeld. Diffusion in Solids, Eds. A. S. Nowick and J. J. Burton, Chap. 5, Academic Press, New York.

[45] K. D. Joppien. Thesis Tech. Univ. Clausthal, Germany (1968).

[46] J. L. Dillard and S. Talbot-Besnard. C.R. Acad. Sci. Ser C 269 1173 (1969).

[47] J. L. Dillard. C. R. Acad. Sci. Ser C 270 669 (1970).

[48] W. Beck, J.O'M Bockris, M.A. Genshaw and P. K. Subaramanyan, Met. Trans. 2 883 (1971).

[49] G. Namboobhiri and L. Nanis. Acta Metall. 21 663 (1973).

[50] H. Veysseyre. Mem. Revue Metall 41 203 (1964).

[51] E. Palczewska and I. Ratyjczyk. Bull Acad. Pol. Sic. Ser. Sci. Chim. 9 269 (1961).

[52] B. Baranowski. Ber. Bunsenges. Phys. Chem. 76 714 (1972).

[53] V. V. Kuznietsov and N. I. Subbonita. Elektronkhimija 1 1906 (1965).

[54] A. Guntherschulze, H. Betz and H. Klemwächter. Z. Phys. 111 657 (1939).

[55] W. Raczynski and S. Talbot-Besnard. C.R. Acad. Sci. Ser C 269 1253 (1969).

[56] W. Dresler and M. G. Frohberg. Jül-Ber, 6th Jül-Conf. (Jülich,Germany) 2 516 (1972

[57] H. G. Ellerbrock, G. Vibrans and H. P. Stuwe. Acta Metall. 20 53 (1972).

[58] A. J. Kumnick and H. H. Johnson. Acta Metall. 25 891 (1977).

[59] J. R. G. da Silva, S. W. Stafford and R. B. McLellan. J. Less-Common Metals 49 407 (1976).

[60] H. Sugimoto and Y. Fukai. Phys. Rev. B 22 670 (1980).

[61] H. K. Birnbaum and G. P. Flynn. Phys. Rev. Lett. 37 25 (1976).

[62] P. S. Flint. General Electric Co. Reports, KAPL-659.

[63] H. Wada and K. Sakamoto. Intern. Fric. Ultrason. Attenuation Solids. Proc. Int. Conf. 6th, 479 (1977).

[64] A. McNabb and P. K. Foster. Trans. AIME 227 619 (1963).

[65] M. Koiwa. Acta Metall. 22 1259 (1974).

[66] M. R. Louthan, P. G. Derrick, J. A. Donovan and G. R. Caskey. Eff. Hydrogen Behav. Mater. Proc. Int. Conf. Moran, Wyoming, AIME, New York, p. 337 (1976).

[67] S. Moriya, S. Takaki and H. Kimura. Mater. Sci. Eng. 32 71 (1978).

[68] R. B. McLellan. Phys. Stat. Sol. (B) 71 K119 (1975).

[69] H. Züchner and N. Boes. Ber. Bunsenges. Phys. Chem. 76 783 (1972).

[70] A. Ferro. J. Appl. Phys. 28 895 (1957).

[71] R. A. Oriani. Hydrogen on Metals, Proc. Conf. Fundamental Aspects of Stress Corrosion Cracking NACE, Houston, 39 (1969).

[72] P. R. Bevington. Data Reduction and Error Analysis for the Physical Science. (1969). McGraw-Hill, New York.

[73] H. Katsuta, R.B. McLellan, and K. Furukawa. J. Phys. Chem. Solids 43 533 (1982).

[74] A. Seeger. Phys. Lett. A 58A, 137 (1966).

[75] R. Handad. Scrip. Met. 11 843 (1977).

[76] G. H. Vineyard. J. Phys. Chem. Sol 3 121 (1957).

[77] C. P. Flynn and A. M. Stonebam. Phys. Rev. 131 3966 (1970).

[78] L. Katz, M. Guinan and R. J. Borg. Phys. Rev. B4, 330 (1971).

[79] J. Crank. The Mathematics of Diffusion. Clarendon, Oxford (1975).

[80] J. P. Redhead, J. P. Hobson and E. V.Kornelson. The Physical Basis of Ultrahigh Vacuum, Chapman and Hill, London (1968).

[81] M. W. Roberts and C. S. McKee. Chemistry of the Metal-Gas Interface (1978), Clarendon, Oxford.

[82] R. Gomer. Interactions on Metal Surfaces 4 (1975). Springer Verlag, New York.

[83] J. A. Anderson. Chemisorption and Reaction on Metal Films (1971), Academic Press, London.

[84] K. Kiuchi and R. B. McLellan. Acta Metall. To be submitted.

[85] D. W. Rudd.and J. B. Ventrano. NAA-SR 6109 (1961).

[86] I. M. Bernstein and A. W. Thompson. Hydrogen in Metals, Americal Society for Metals (1973).

[87] A. W. Thompson and I. M. Bernstein. Effect of Hydrogen on Behavior of Materials (1975), AIME, New York.

[88] Y. Yamakawa, T. Tsuruta and Y. Yoshizawa. J. Boshoku Gijutsu 30 501 (1981).

[89] V. I. Shapovolov and L. M. Poltoratski. Izv. Vyssh. Uchebn Zaved Chern Metall. 10 124 (1978).

[90] R. B. McLellan. Scripta Met. 15, 1251 (1981).

[91] J. P. Hirth and B. Carnaham. Acta. Metall. 26 1795 (1978).

[92] I. G. Ritchie, J. F. Dufrensue and P. Moser. Phys. Stat. Sol. A 52 331 (1979).

Table 1 Comparison of Representative Measurement Method for the Permeation of Hydrogen in Metals.

METHOD	TYPE	PRINCIPLE	TECHNIQUE	CHARACTERISTICS	DETECTION LIMIT (ppm)
H_2-Gas Equilibration	Steady State	Permeation	Pressure Change	Most Convenient Method	1
		Desorption	Volume Change	Sealing Solvent(Hg,Silicone Oil,Glyceline et.al.)	10^{-1}
	Transient	Time-Lag	Lawrence Gage	Ionization of Hydrogen Atom	10^{-3}
		Absorption	Gas Chromatography and Mass Spectrometry	Most Quantitative Method	10^{-5}
Electrochemical	Conventional Permeation	Surface Potential	Cathodic Current Control and Measurement for Change of Electrochemical Potential on The Other Side.	Metals Having High Diffusion Coefficient and High Hydrogen Solubility. Low Temp.	1
	Two Sided Extraction	Hydrogen Discharge	Bielectrode(Galvanic Cell and Potentiostatic Cell) - Anodic Current Measurement	Simultaneously Quantitative Measurements for Diffusion Coefficient and Solubility Low Temp.	10^{-2}
Surface Independent	Elastic Properties	Gorsky Effect		Low Temp.	~
	Metallographic Change	Aging-Recovery	Electrical Resistivity Magnetic Measurement etc.	Limitation of Specimen Materials	Depends on Materials
	Direct Observation of Penetration Profile	Radioactive Tracer	Radiochemical Effect	Special H^3 Handring Technique Demanded	Depends on Detection Method
		Sputtering-Depth Profile	IMMA or SIMS	Sensitivity is High	$\sim 10^{-5}$

Table 2 Diffusion Coefficients for Hydrogen in α Iron.

Method		Activation Energy Q, KJ/mol.	Prefrequency Factor Do, m^2/s	Temperature Range °C	Measurement Techniques	Specimen Purity	Reference No. & Sign on Fig.1 Researcher, year, No. Sign
H_2-Gas Equilibration Technique	Pd-Coated UHV Method	6.70	1.01×10^{-7}	69～346	Permeation	99.9	Miller(1975) (2) PC2
		6.70	2.30×10^{-7}	47～560	Permeation	Z.R.	Nelson(1972) (3) PC3
		7.07	1.61×10^{-7}	49～506	Permeation	Z.R.	Quick(1978) (4) PC4
	Steady-State Method	9.54	7.60×10^{-8}	20～800	Permeation		Sykes(1947) (5) P5
		10.80	1.02×10^{-7}	550～900	Permeation	99.9	Schenk(1959) (6) P6
		12.10	2.17×10^{-7}	400～900	Permeation	P.I.	Geller(1950) (7) P7
		5.86	4.74×10^{-8}	326～816	Desorption		Domke(1971) (8) D8
		6.03	2.14×10^{-8}	25～300	Desorption		Koenig(1975) (9) D9
		6.53	4.95×10^{-8}	298～878	Desorption	P.I.	Maas(1958) (10) D10
		7.70	～	200～700	Desorption		Erdmann(1969) (11) D11
		8.04	6.42×10^{-8}	300～900	Desorption	99.98	Heumann(1966) (12) D12
		9.17	6.70×10^{-8}	430～725	Desorption		Carmichael(1960) (13) D13
		11.3	9.30×10^{-8}	200～774	Desorption	A.I.	Eichenauer(1958) (14) D14
		12.8	8.85×10^{-8}	150～900	Desorption	99.96	Stross(1956) (15) D15
		13.4	1.40×10^{-7}	200～780	Desorption	99.9	Johnson(1960) (16) D16
		16.1	1.20×10^{-7}	25～900	Desorption		Zitter(1958) (17) D17
		22.4	3.65×10^{-7}	25～650	Desorption		Lee(1961) (18) D18
		32.7	1.20×10^{-5}	25～200	Desorption	99.9	Johnson(1960) (19) D16'
		35.6	1.10×10^{-6}	10 ～ 70	Desorption	99.956	Evans(1969) (19) D19
		36.2	1.70×10^{-5}	23 ～ 84	Desorption	99.67	Evans(1969) (19) D19'
		40.8	5.10×10^{-5}	23 ～ 84	Desorption	98.6	Evans(1969) (19) D19"
	Transient Method	4.52	3.87×10^{-8}	126～693	Transient	99.9	Bryan(1969) (20) T20
		13.0	2.20×10^{-7}	10～100	Transient		Choi(1970) (21) T21
		13.7	1.42×10^{-7}	209～600	Transient	99.8	Wagner(1964) (22) T22
		13.8	2.20×10^{-7}	30 ～ 90	Transient		Raczynski(1961) (23) T23
		15.1	1.10×10^{-6}	80～180	Transient	99.8	Wach(1966) (24) T24
		17.6	3.80×10^{-7}	80～300	Transient		Chene(1977) (25) T25
		24.8	6.10×10^{-6}	15 ～ 60	Transient	Iron A	Reiermann(1970) (26) T26
		27.2	6.50×10^{-6}	15 ～ 60	Transient	Iron B	Reiermann(1970) (26) T26'
		36.5	1.10×10^{-6}	23 ～ 80	Transient		Barrer(1940) (27) T27
		69.1	$1.70 \times 10^{+1}$	25 ～ 80	Transient		Chene(1977) (25) T25'
		14.3	5.00×10^{-8}	26 ～ 90	Absorption		Frank(1958) (28) T28
Electrochemical Technique		4.86	6.20×10^{-8}	10 ～ 70	Ni-Coated	Single	Yamakawa(1981) (29) E29
		5.57	6.00×10^{-8}	10 ～ 75	Pd-Coated	A.I.	Beck(1966) (30) E30
		5.57	6.00×10^{-8}	10 ～ 90	Pd-Coated	A.I.	McBreen(1965) (31) E31
		6.70	1.10×10^{-7}	-43 ～ 27	Pd-Coated	Single	Hagi(1978) (32) E32
		7.03	～	10 ～ 60	Pd-Coated	99.996	Raczynski(1978) (33) E33
		7.49	1.05×10^{-7}	5 ～ 80	Pd-Coated		Asano(1971) (34) E34
		9.21	2.50×10^{-6}	10 ～ 70		99.99	Subramanyan(1971) (35) E35
		17.6	1.40×10^{-6}	5 ～ 60	Pd-Coated	99.8	Kumnick(1974) (36) E36
		18.8	～	40 ～ 90			Mindyuk(1973) (37) E37

P.I. ; Pure Iron , A.I. ; Armco Iron , Z.R. ; Zone Refined

Table 3 Values measured by Representative Measurement Techniques.

REGION	MEASUREMENT METHOD	TEMPERATURE RANGE °C	MOST PROBABLE VALUE BY STATISTICAL ANALYSIS ACTIVATION ENERGY KJ/mol	PREFREQUENCY FACTOR m^2/s	RATE DETERMINING STEP ON MEASUREMENT	NUMBER OF SAMPLING REPORTS
A *	Pd Coated, UHV (H_2 Gas Equilibration)	50～550	6.70～7.12	1～2.5 x 10^{-7}	Bulk Diffusion of Hydrogen	3
B	Electrochemical	-40～80	5.69	7.23 x 10^{-8}	Bulk Diffusion of Hydrogen	20
C **	H_2-Gas Equilibration (Bare Metal)	25～900	8.37	6.70 x 10^{-8}	Surface Reaction (Desorption of Hydrogen)	24
D	Data obtained from Specimens Containing Defects or Surface Trapping Sites which Produced Unsatisfactory Results.					15

* Statistical analysis not performed.

** This method incorporates following techniques:
Major Data ; Steady State Method(Permeation, Desorption)
Minor Data ; Transient Method(Time-Lag Type Permeation, etc.)

Table 4 Apparent Diffusivity at $t \to \infty$ Corresponding to Surface Reaction Conditions (Crank[79])

SURFACE REACTION	FICK'S SECOND LAW	SURFACE BOUNDARY CONDITION, C_s	GENERAL EQUATION OF PERMEATION RATE, F=	APPARENT DIFFUSION COEFFICIENT AT $t \to \infty$
None	$(\partial C/\partial t)=D(\partial^2 C/\partial x^2)$	$C_s=0$	DC_o	D
Reversible 1st Order Reaction (Immobilized Reactant)	$(\partial C/\partial t)=D(\partial^2 C/\partial x^2)-(\partial C_s/\partial t)$	$C_s=k_1 C$	$[D/(k_1+1)]C_o$, $k_1=f(t)$	$D/(k_1+1)$
		$C_s=k_n C^n$ $(n>1)$	Effective Diffusion Coefficient is not Constant $(C_s/t)=-\frac{}{x}[(D/N)(1/k_n)^{1/n}C_s^{(1-n)/n}](\partial C_s/\partial x)$	Depend on n and Reaction Type
Irreversible 1st Order Reaction	$(\partial C/\partial t)=D(\partial^2 C/\partial x^2)-k_1 C$	$C_s=C_o^s$ $(t>t_1)$	$C_o(Dk_1)^{1/2}\mathrm{erf}(k_1 t)^{1/2}+\exp(-k_1 t)/(\pi k_1 t)^{1/2}$ kt ; Small , $C_o(1+k_1 t)[D/(\pi t)]^{1/2}$	$(Dk_1)^{1/2}$
		$C_s=h(C_o^s-C)$ $(h=K_1/D)$ $t>0$	$[hDC_o/(h^2D-k_1)][h(Dk_1)^{1/2}\mathrm{erf}(k_1 t)^{1/2}+h^2D\ \mathrm{erf}[h(Dt)^{1/2}]\exp[t(h^2D-k_1)]-k_1]$	$hD/(1+h(D/k_1))^{1/2}$

Where C_o^s ; Extapoiated value for infinite time, C_s ; Real surface concentration of hydrogen.

k_n ; Rate constant for surface reaction (first-order k_1, n-order k_n, etc.)

D ; Diffusion Coefficient for hydrogen in bulk.

C_o ; Solubility for hydrogen in bulk at the gas input surface.

h ; k_1 / D, t_1 = time to reach steady state.

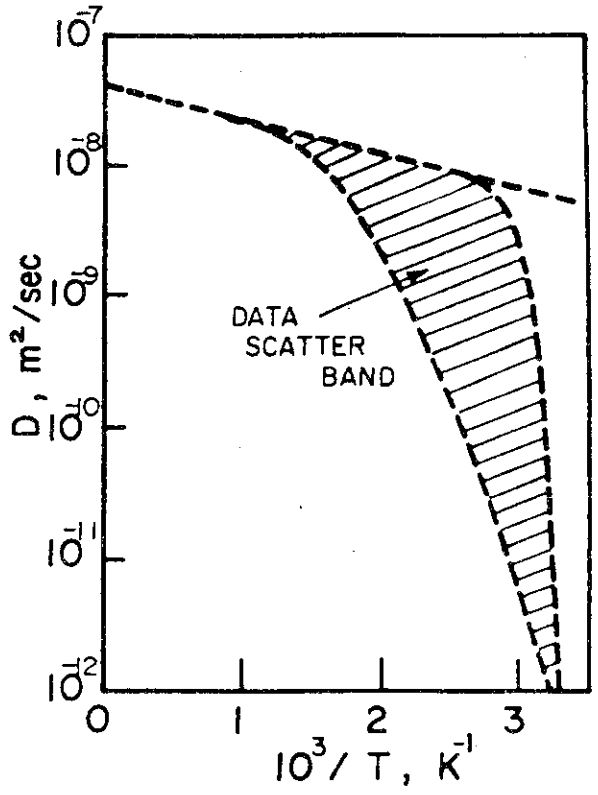

Fig.(1) Approximate data scatter band encompassing 36 individual H-diffusivity measurement sets for well-annealed iron.

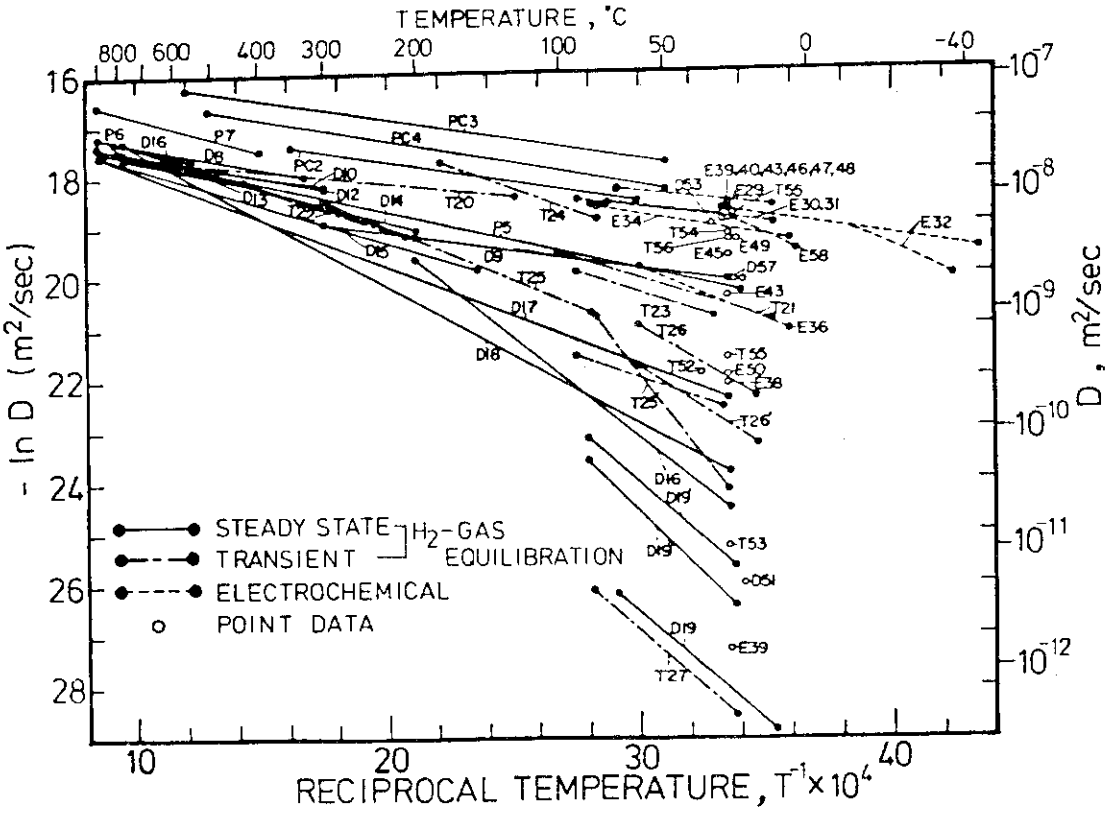

Fig.(2) Arrhenius representation of the current data for the diffusion of hydrogen through BCC iron.

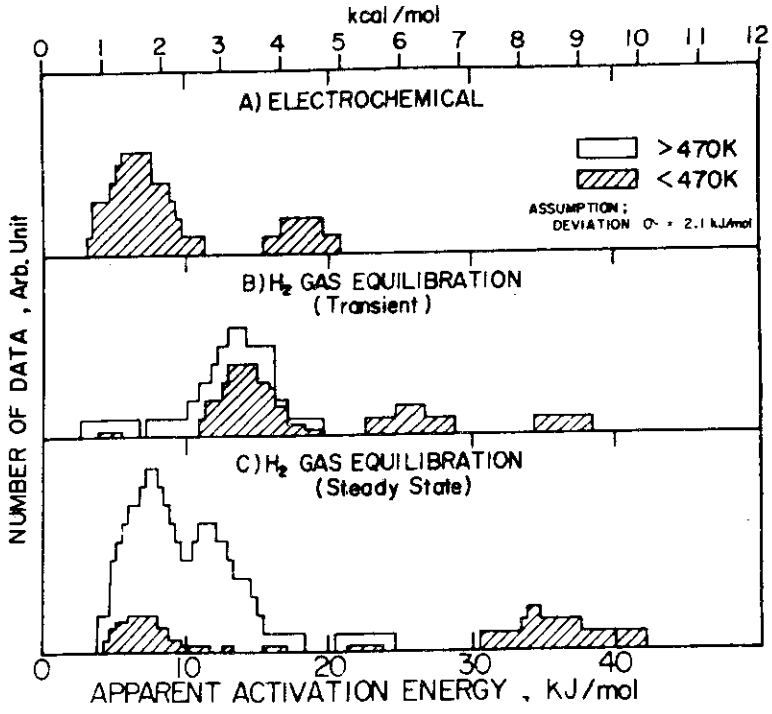

Fig.(3) Histograms of the apparent H-diffusion activation energies in BCC iron. The three part diagrams refer to differing experimental techniques.

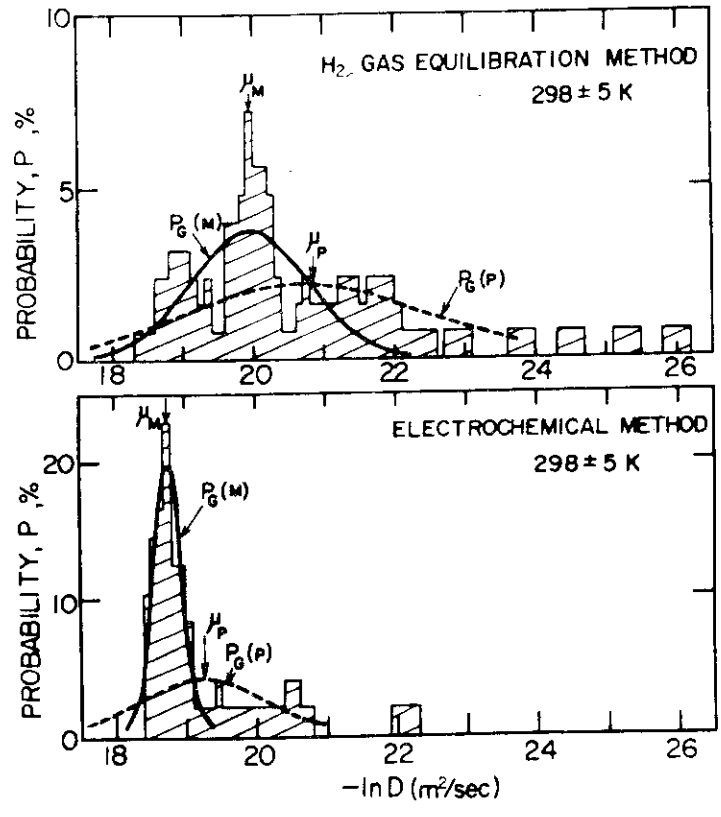

Fig.(4) Probability (P_G) histograms of -ln D for the data taken from H_2 gas equilibration experiments for the H-diffusivity in BCC iron (upper diagram) and from electrochemical determinations (lower diagram). The reference temperature is 298 ± 5 K.

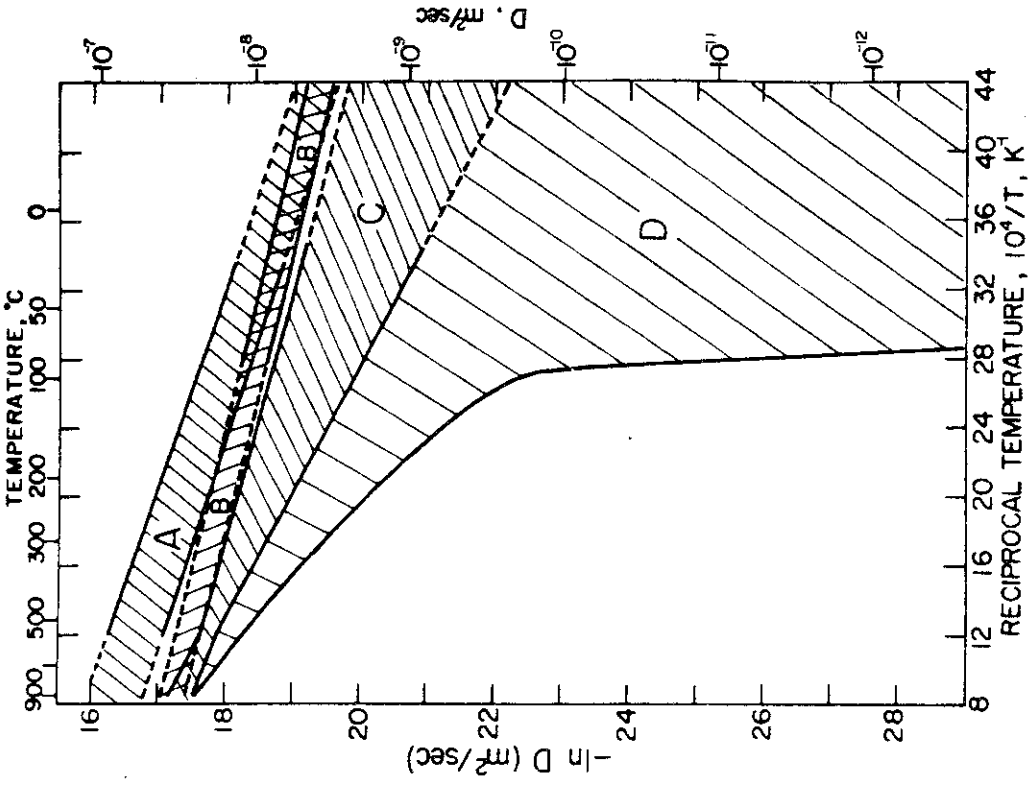

Fig.(6)
Results of the statistical data analysis. Each region A, B, C and D corresponds to differing experimental or sample preparation conditions as discussed in the text.

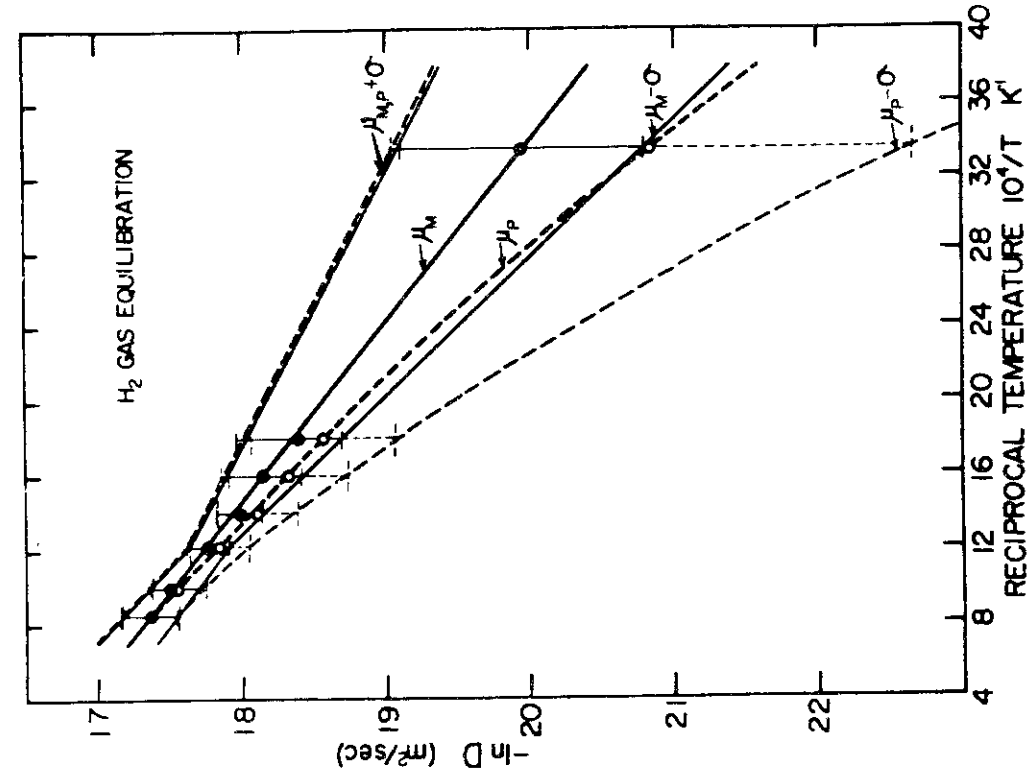

Fig.(5)
The most probable values (corresponding to $P_G(M)$) of -ln D taken from H_2 gas equilibration experiments plotted against reciprocal temperature (symbol ●). The -symbols give the values caluculated from equ.(2), i. e. corresponding to $P_G(P)$. The -ln D values taken from $P_G(M)$, and their error band + are in solid lines and the -ln D values corresponding to $P_G(^{H}P)$ and their error are connected by dashed lines.

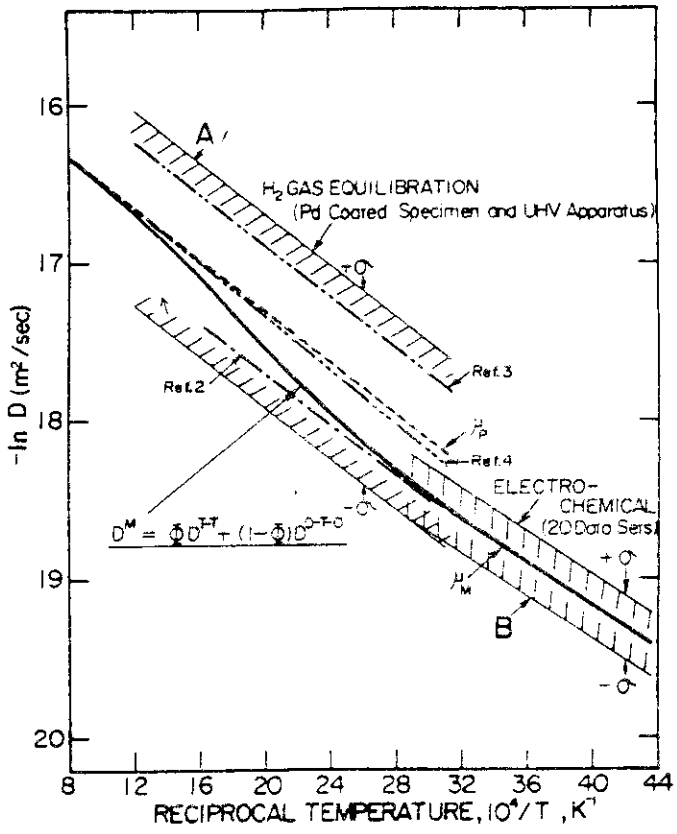

Fig.(7) Best values of the data taken from regions A and B of Fig.(6) The lower (B) region (——·——) repesents the best values taken from 20 data sets using the electrochemical method (table III) and each of the three data sets of region A are shown by individual lines (see inset in Fig.(7)) and their weighted average (-----).

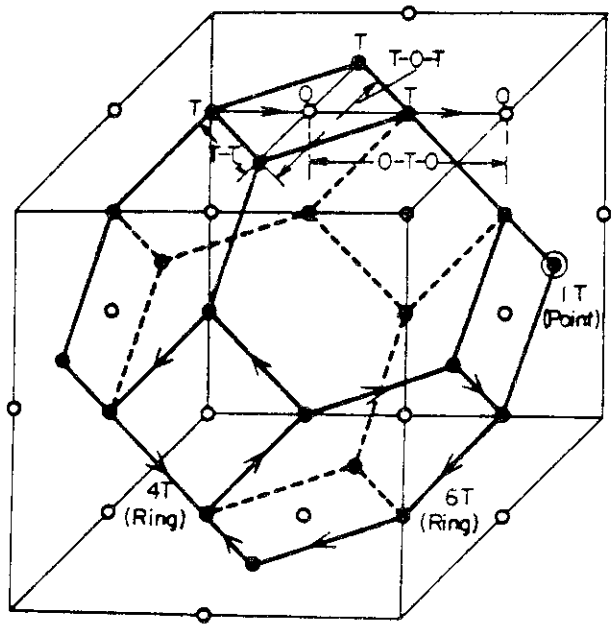

Fig.(8) Representation of octahedral (O) and tetrahedral (T) sites in the BCC lattice. The T-T, O-T-O and T-O-T jump paths and 4T and 6T " ring " jump path are also depicted.

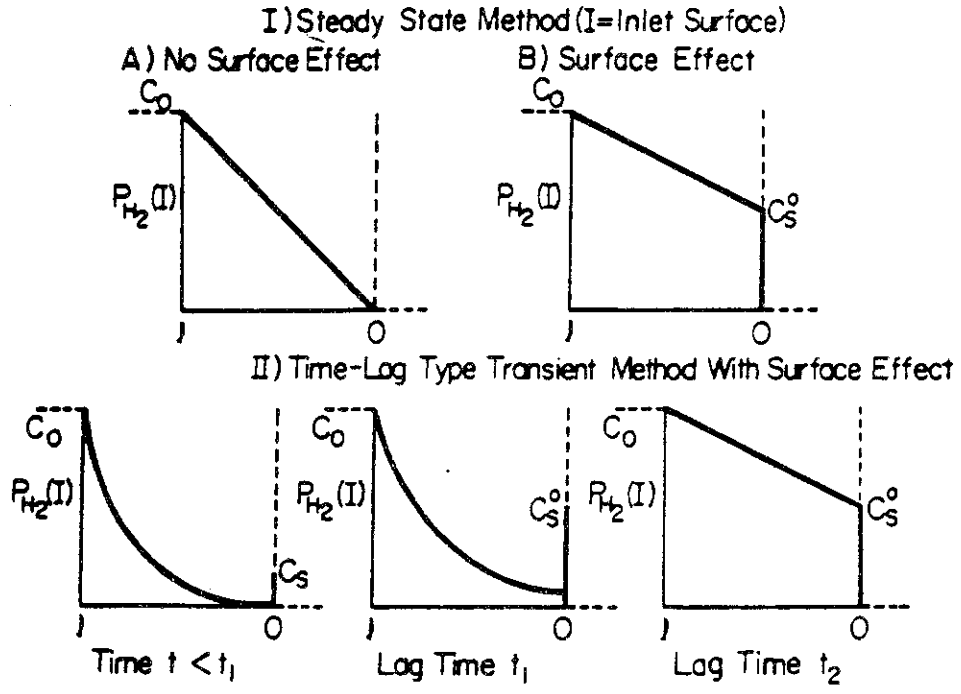

Fig.(9) Graphical representations of the H concentration profiles (I = inlet surface), for the steady state method with (A) and without (B) surface reactions. The lower diagram represents the profiles for the transient method with a surface reaction at early times ($t < t_1$), t_1 and at a time t_2 such that the outret H concentration C_s has reached its steady state value (see Crank, [79]).

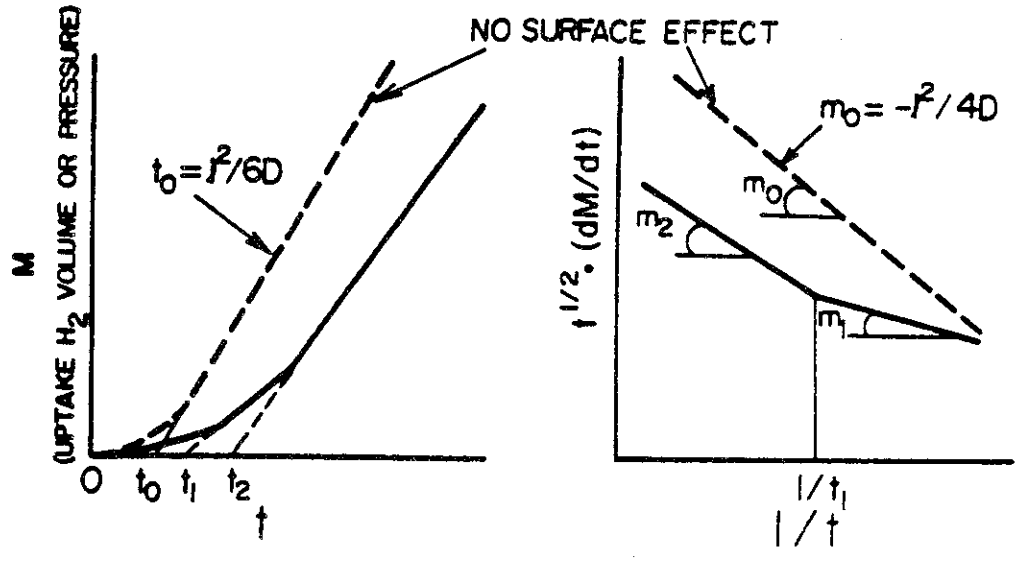

Fig.(10) Slopes of the outlet rate of H as a function of time obtained in the transient (time-lag) method. The different slopes correspond to the times t_i as shown in the profile diagrams in the lower part of Fig.(9).

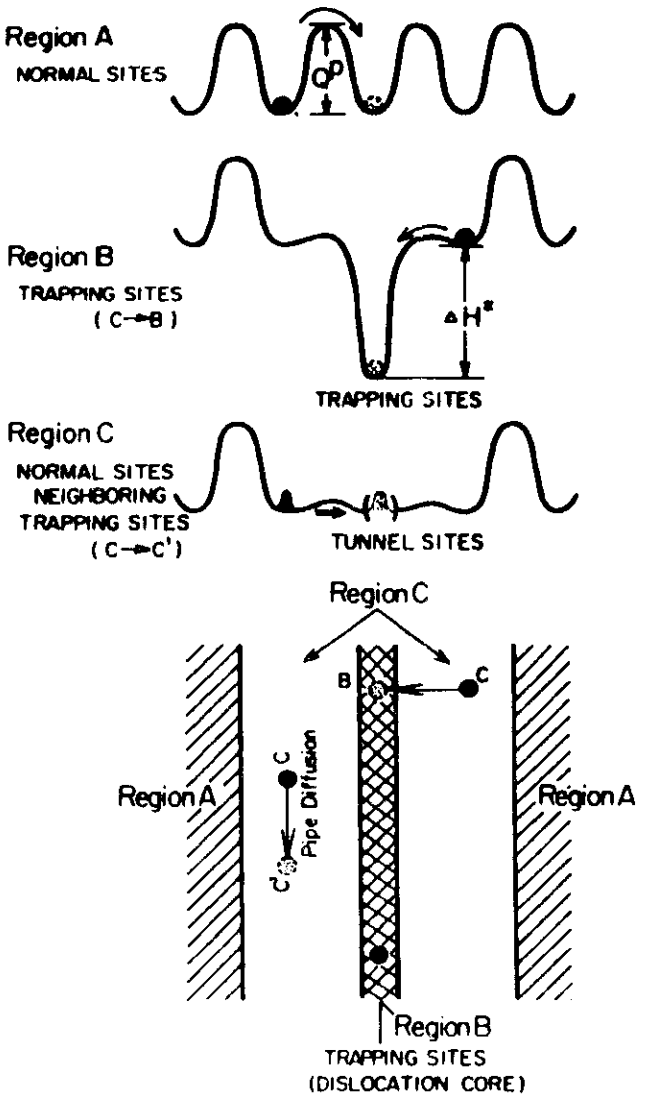

Fig.(11)

Energy minima and saddle point energies in the BCC lattice. The upper diagram depicts classical hopping by the T-T mechanism. The center diagram shows sites adjacent to trapping sites and the lower diagram " tunnel " sites for pipe diffusion along dislocation lines.

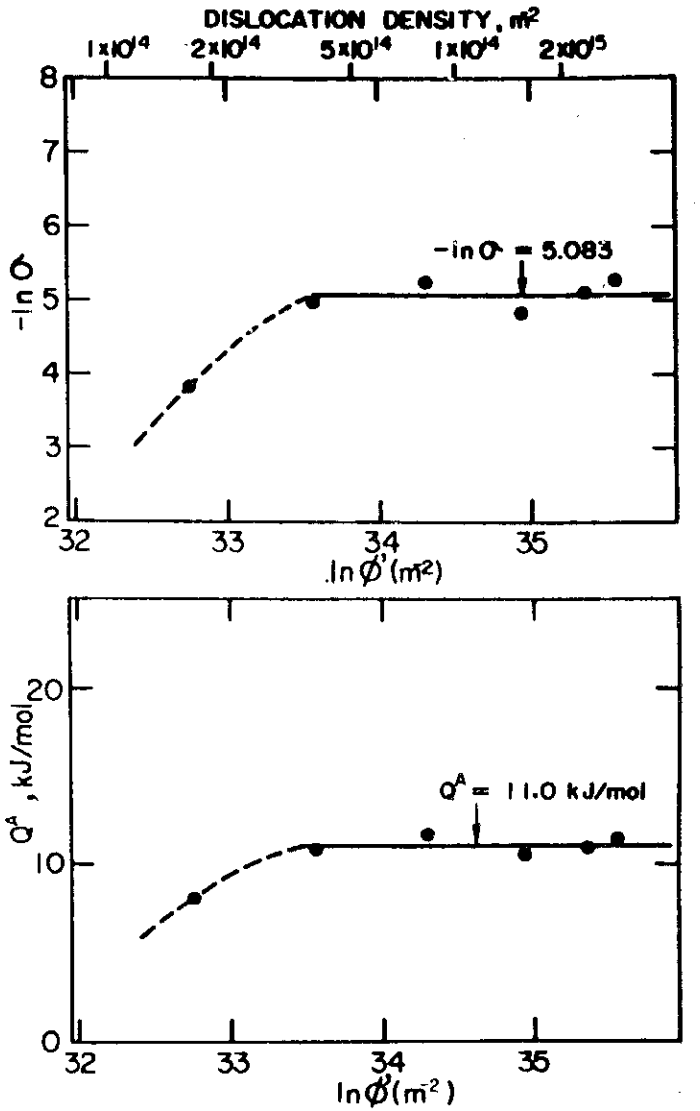

Fig.(12)

Estimation of the quantities and Q^A from diffusivity measurements for H in iron single crystals and deformed iron.

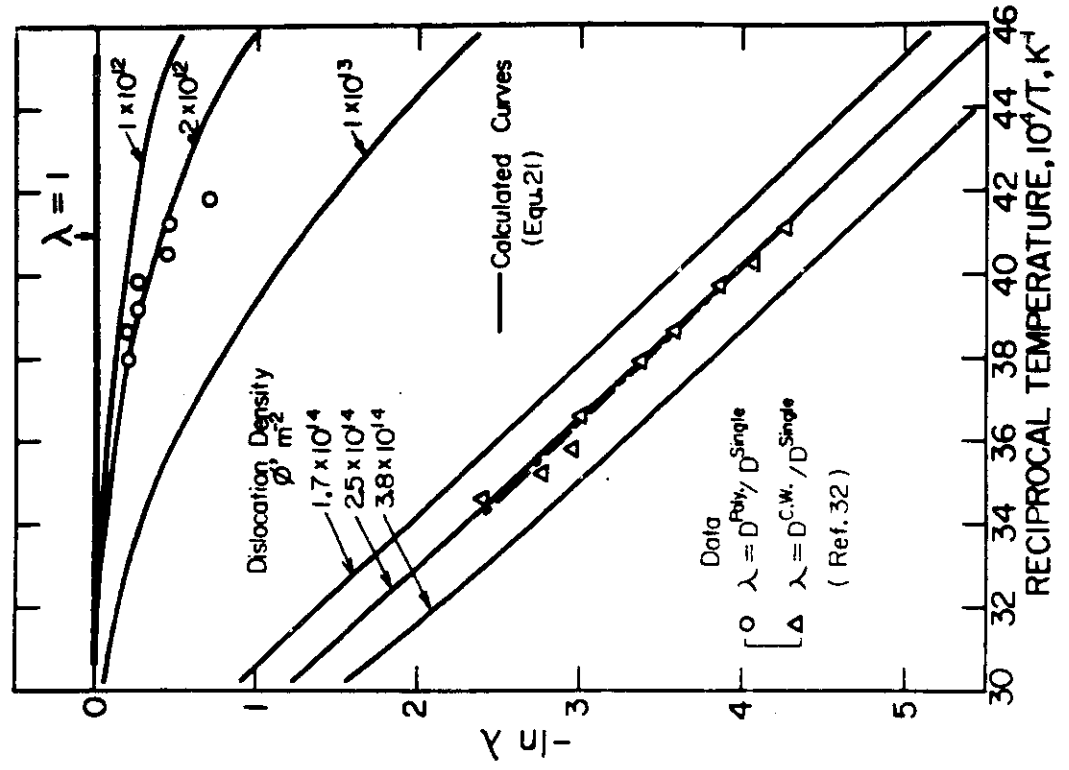

Fig.(14)
Diffusivity ratio (λ) for deformed (Δ) and non-deformed (o) polycrystalline iron as a function of reciprocal temperature compared with caiculated values (solid lines).

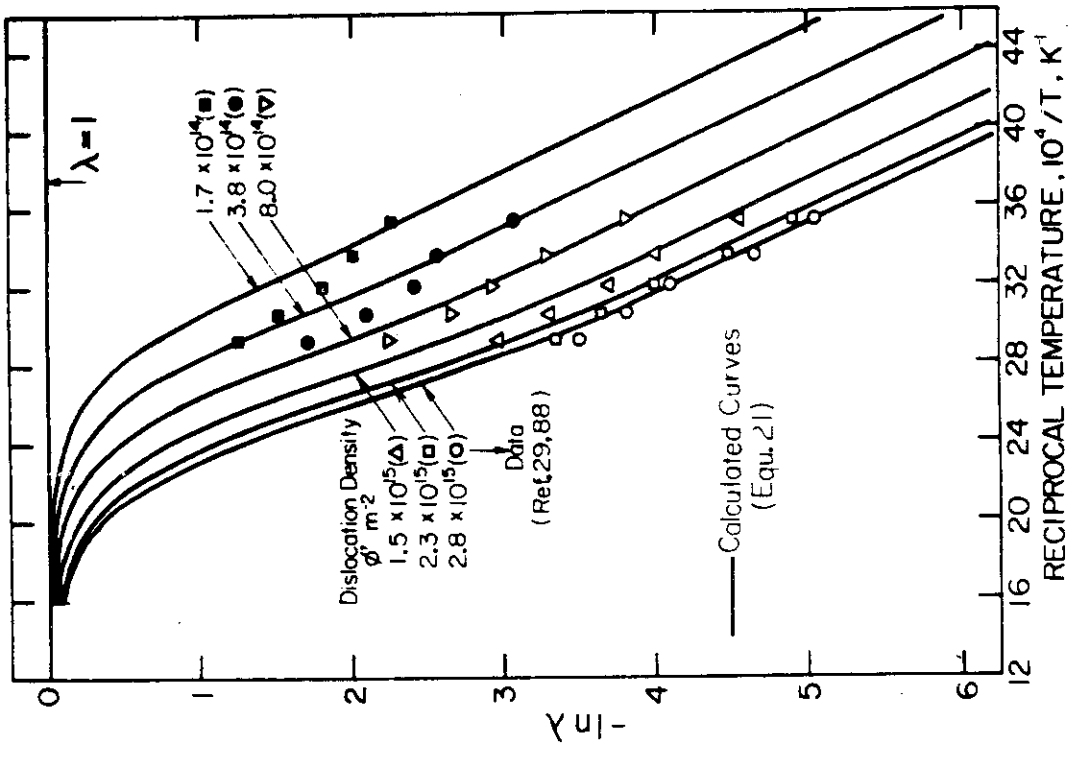

Fig.(13)
Diffusivity ratios (λ) as a function of reciprocal temperature for different dislocation densities ' taken from experiment (point symbols) and calculated values (solid lines).

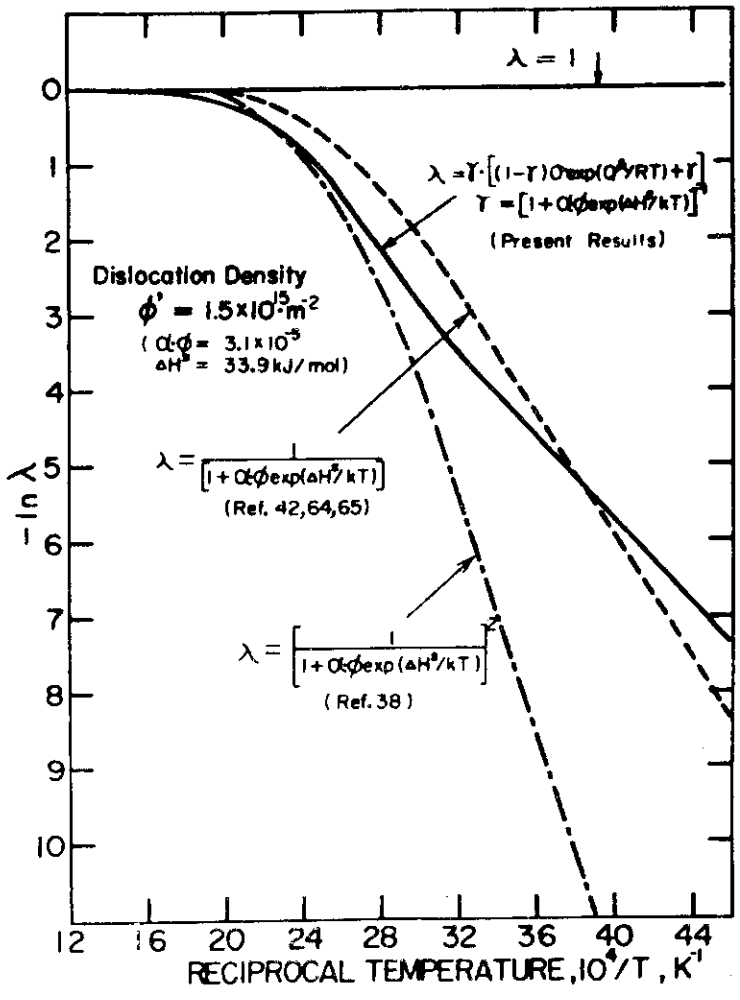

Fig.(15) Comparison of the diffusivity ratio $\lambda = D_{eff}/D_L$ calculated from various trapping models concomitant to a trap depth of 33.9 kJ/mol and dislocation density of 1.5×10^{15} m^{-2}.

謝　　辞

本研究にあたり，御指導下さいました，Rice 大学Prof．Rex B．McLellan 教授ならびに経済的な援助を頂いたRobert A．Welch FoundationならびにU．S．Departments of Energy に心から謝意を表する。